

Large-scale simulations of Floquet physics on near-term quantum computers

Timo Eckstein,^{1,2,3,*} Refik Mansuroglu,¹ Piotr Czarnik,^{4,5} Jian-Xin Zhu,^{3,6} Michael J. Hartmann,^{1,2} Lukasz Cincio,³ Andrew T. Sornborger,^{7,†} and Zoë Holmes^{3,8,‡}

¹*Department of Physics, Friedrich-Alexander Universität Erlangen-Nürnberg, Erlangen, Germany*

²*Max-Planck Institute for the Science of Light, Erlangen, Germany*

³*Theoretical Division, Los Alamos National Laboratory, Los Alamos, New Mexico 87545, USA*

⁴*Faculty of Physics, Astronomy, and Applied Computer Science, Jagiellonian University, Kraków, Poland*

⁵*Mark Kac Center for Complex Systems Research, Jagiellonian University, Kraków, Poland*

⁶*Center for Integrated Nanotechnologies, Los Alamos National Laboratory, Los Alamos, New Mexico 87545, USA*

⁷*Information Sciences, Los Alamos National Laboratory, Los Alamos, New Mexico 87545, USA*

⁸*Laboratory of Quantum Information and Computation,*

École Polytechnique Fédérale de Lausanne, Lausanne, Switzerland

Quantum systems subject to periodic driving exhibit a diverse set of phenomena both of fundamental and technological interest. However, such dynamical systems are more challenging to simulate classically than their equilibrium counterparts. Here, we introduce the Quantum High Frequency Floquet Simulation (QHFFS) algorithm as a method for simulating the dynamics of fast-driven Floquet systems on quantum hardware. Central to QHFFS is the concept of a kick operator which transforms the system into a basis where the dynamics is governed by a time-independent effective Hamiltonian. This allows prior methods for time-independent Hamiltonian simulation to be lifted to the simulation of Floquet systems. We use the periodically driven biaxial next-nearest neighbor Ising (BNNNI) model as a case study to illustrate our algorithm. This oft-studied model is a natural test bed for quantum frustrated magnetism and criticality. We successfully implemented a 20-qubit simulation of the driven two-dimensional BNNNI model on Quantinuum’s trapped ion quantum computer. This is complemented with an analysis of QHFFS algorithmic errors. Our study indicates that the algorithm exhibits not only a cubic scaling advantage in driving frequency ω but also a linear one in simulation time t compared to Trotterisation, making it an interesting avenue to push towards near-term quantum advantage.

I. Introduction

There has been a recent spike of interest in the dynamical control of quantum phases by driving strongly correlated quantum systems out of equilibrium. In particular, Floquet systems, that is quantum systems subjected to periodic driving, not only exhibit a rich set of physical phenomena, including exotic non-equilibrium topological phases of matter [1–6], but can also generate quantum phenomena on demand for technological applications [7–11]. For example, time crystalline phases [12], which break continuous time-translational symmetry have been demonstrated with trapped ions [13], superconducting qubits [14–16] and diamond defects [17]. Similarly, periodic driving can lead to symmetry-protected edge modes [2, 3, 6, 18], a phenomenon that has been realized in both trapped ions [19] and superconducting [20] platforms, and has potential applications for error correction. However, the strong correlations present in such systems make their modelling classically challenging.

The potential of simulating the dynamics of quantum systems exponentially more efficiently than is possible classically provided one of the original motivations for developing quantum hardware [21–23]. While a distant

dream for decades, with rapid technological progress, the possibility of realising a quantum advantage for quantum simulation is now in sight [24, 25]. Nonetheless, error rates are yet to reach the error correction threshold for moderate-sized devices and hence quantum simulation algorithms designed for fault-tolerant devices remain challenging for the near future [26–30]. This has prompted the search for quantum simulation algorithms suitable for implementation on near-term quantum devices [28, 31–43]. However, most of these studies focused on simulating time-independent systems and less attention has so far been paid to how to simulate periodically driven systems.

Standard Trotterization [1–6, 12–20, 44–49], where the time-ordered integral governing the dynamics is discretized into short time-steps (implemented via a Trotter approximation), fails to take advantage of the periodic structure of Floquet problems and thus acquires a substantial computational overhead. Alternative proposals include solving the Schrödinger-Floquet equation [46, 50] and using variational optimization [47]. The former requires fault-tolerant techniques and the latter is limited by (noise-induced) barren plateaus [51–58] as well as other barriers to variational optimization on near-term quantum hardware [59–61]. Correspondingly, digital quantum simulations of systems subject to a continuous driving field have thus far been limited to only a few qubits [48, 49].

Here we draw motivation from prior work on classical methods for studying Floquet physics [62–68] and

* Timo.Eckstein@fau.de

† sornborg@lanl.gov

‡ zoe.holmes@epfl.ch

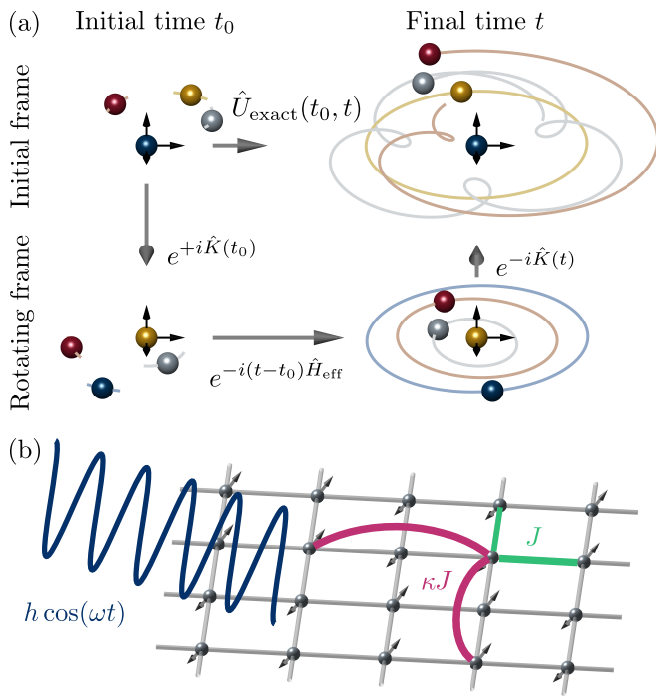


FIG. 1. **Method overview.** (a) QHiFFS Algorithm Concept. To realize a time-dependent periodic time evolution, we transform from the standard basis to a (periodically) rotating frame using $e^{+i\hat{K}(t_0)}$. Evolution in this frame from t_0 to t is governed by the time-independent effective Hamiltonian \hat{H}_{eff} . The adjoint of the kick operator $e^{-i\hat{K}(t)}$ is applied at the final simulation time t to kick back into the original frame. (b) Benchmark system. To demonstrate the advantage of QHiFFS, as compared to standard Trotterization, we implement the 20-qubit transversely driven 2D biaxial next-nearest neighbor Ising (BNNNI) model with periodic boundary conditions on Quantinuum’s H1 trapped ion quantum hardware (see Fig. 3). The BNNNI model, Eq. (8), consists of nearest-neighbour coupling with strength J and next-nearest-neighbour coupling with strength κJ . We suppose a 4 by 5 qubit lattice is periodically driven with strength h and at frequency ω .

methods for analogue quantum simulation [44], to develop a new quantum algorithm for simulating periodically driven systems on digital quantum computers. Crucially this approach takes explicit advantage of the periodicity of the driving terms to reduce the resource requirements of the simulation. Key to our approach, is the use of a high-frequency approximation that performs a time-dependent basis transformation into a rotating frame [65]. This transformation, which can be implemented on quantum hardware using a *kick operator*, allows one to transform a time-dependent quantum simulation into a time-independent one. Previously developed time-independent techniques can then be lifted and reused for the Floquet simulation [26–35]. The Quantum High Frequency Floquet Simulation (QHiFFS – pronounced *quiffss*) algorithm thus opens up the potential of simulating fast-driven systems using substantially

shorter-depth circuits than standard Trotterisation.

We use QHiFFS to implement a 20-qubit two-dimensional simulation of the transversely driven biaxial next-nearest neighbor Ising (BNNNI) model on a trapped ion quantum computer. This implementation is, to the best of our knowledge, the largest digital 2D quantum simulation of a periodically driven system to date (see Sec. III). We choose to focus on the BNNNI model because it is one of the most representative spin-exchange models containing both tunable frustration and tunable quantum fluctuations, creating competing quantum phases and criticality. Indeed, this behaviour is successfully captured by our hardware implementation. We stress that this simulation would not have been feasible using standard Trotterisation, which would have required a 50-fold deeper circuit (see Fig. 3).

Finally, we set QHiFFS on solid analytic foundations by providing an analysis on the scaling of the final simulation errors. In particular, we find that first order QHiFFS not only exhibits a cubic scaling advantage in driving frequency ω , but also a linear one in simulation time t compared to a second order Trotter sequence. The scaling in system size n remains linear for local models (see Sec. III C). Thus we see QHiFFS finding use both on moderate-sized error-prone near-term devices and in the fault tolerant era.

II. The QHiFFS Algorithm

The QHiFFS algorithm simulates quantum systems governed by a Hamiltonian of the form

$$\hat{H}(t) = \hat{H}_0 + \hat{V}(t) \quad \text{with} \quad \hat{V}(T+t) = \hat{V}(t), \quad (1)$$

where \hat{H}_0 is the time independent non-driven Hamiltonian and $\hat{V}(T+t)$ is a periodic driving term. Without loss of generality the driving term can be expanded in terms of its Fourier components $\hat{V}^{(j)}$ as

$$\hat{V}(t) = \sum_{j=1}^{\infty} \hat{V}^{(j)} e^{ij\omega t} + \hat{V}^{(-j)} e^{-ij\omega t}. \quad (2)$$

where $\omega = 2\pi/T$ is the driving frequency. Here we focus on the limit where the driving frequency is large, that is (in broad terms) when $\omega \gg \|\hat{H}_0\|_{\infty}$ and $\omega \gg \|\hat{V}_j\|_{\infty}$. Our aim is to simulate real time evolution under this Hamiltonian from some initial time t_0 to some final time t . That is, to implement the unitary

$$\hat{U}_{\text{exact}}(t_0, t) = \mathcal{T} \exp \left(-i \int_{t_0}^t \hat{H}(t) dt \right), \quad (3)$$

where \mathcal{T} is the time ordering operator.

As is often found in physics, choosing the right reference frame is key to a simple description of the dynamics of a system. To take a paradigmatic example - the motion of planets in our solar system appears rather complex in the earth’s reference frame but becomes much

simpler if we transform into the frame of reference of the sun. Our algorithm, as sketched in Fig. 1, takes a similar approach [69, 70]. Namely, we use a time-dependent *kick operator*, $\hat{K}(t)$, to transform the system to a frame of reference where the dynamics of the driven system is governed by a time-independent *effective Hamiltonian*, \hat{H}_{eff} .

More concretely, the total simulation is composed of the following steps:

1. We apply $e^{+i\hat{K}(t_0)}$ to *kick* an initial state $|\psi\rangle$ at time t_0 into our preferred reference frame.
2. We apply $e^{-i(t-t_0)\hat{H}_{\text{eff}}}$ to evolve the state from times t_0 to t in this new reference frame.
3. We apply $e^{-i\hat{K}(t)}$ to *kick* the system back into the original (lab) frame of reference.

Or, more compactly, the total simulation is of the form

$$\hat{U}_{\text{exact}}(t_0, t) = e^{-i\hat{K}(t)} e^{-i(t-t_0)\hat{H}_{\text{eff}}} e^{+i\hat{K}(t_0)}. \quad (4)$$

Crucially, as previously claimed, \hat{H}_{eff} is time-independent. Thus, one can use prior methods [26–35] for time-independent quantum simulation for its implementation. Furthermore, in many cases, as discussed below, the kick operator, $\hat{K}(t)$, will take a simple form enabling it to be easily implemented on quantum hardware.

The appropriate kick transformation and corresponding effective Hamiltonian for a periodically-driven system, Eq. (1), were derived in Ref. [65] by expanding the kick operator and effective Hamiltonian in powers of the driving frequency as

$$\hat{K}(t) = \sum_{k=1}^{\infty} \frac{1}{\omega^k} \hat{K}^{(k)}(t) \quad \text{and} \quad \hat{H}_{\text{eff}} = \sum_{k=0}^{\infty} \frac{1}{\omega^k} \hat{H}_{\text{eff}}^{(k)}. \quad (5)$$

As explained in detail in Appendix B 1, by first substituting Eq. (5) into Eq. (4) and effectively comparing with Eq. (3) (using Hadamard’s lemma), one can iteratively identify the terms $\hat{K}^{(k)}(t)$ and $\hat{H}_{\text{eff}}^{(k)}$ by associating time-independent terms with $\hat{H}_{\text{eff}}^{(k)}$ and time-dependent ones with $\hat{K}^{(k)}(t)$. In particular, truncating at $\mathcal{O}(\frac{1}{\omega^2})$, the effective Hamiltonian \hat{H}_{eff} and kick operator $\hat{K}(t)$ are given by:

$$\hat{H}_{\text{eff}} \approx \hat{H}_0 + \frac{1}{\omega} \sum_{j=1}^{\infty} \frac{1}{j} [\hat{V}^{(j)}, \hat{V}^{(-j)}] \quad (6)$$

$$\hat{K}(t) \approx -\frac{i}{\omega} \sum_{j=1}^{\infty} \frac{1}{j} \left(\hat{V}^{(j)} e^{ij\omega t} - \hat{V}^{(-j)} e^{-ij\omega t} \right) \quad (7)$$

For expressions for \hat{H}_{eff} and $\hat{K}(t)$ at higher orders, see Appendix B. We note that the rotating wave approximation takes an analogous approach in the sense that under the rotating wave approximation evolution is governed

by the 0th order approximation to the propagator in the interaction picture.

The resources required to implement a simulation via the QHiFFS algorithm depend on the forms of $\hat{V}(t)$ and \hat{H}_0 . Here we describe a physically motivated setting in which the final simulation is particularly simple. A more detailed account of the resources required for other cases is included in Appendix B 2.

In what follows, we will focus on local driving (i.e., assume $\hat{V}(t)$ is one-local). This is a natural limit to consider since many driving phenomena, for example the optical driving of lattice systems, can be modeled in terms of local driving. In this case, $\hat{K}(t)$ is one-local to second order. Thus the initial and final kicks in Eq. (4) can be implemented using only single qubit rotations. If we further assume that $\hat{V}^{(j)}$ and $\hat{V}^{(-j)}$ commute for all j , which is the case here, then the first order correction to \hat{H}_{eff} vanishes and we have that $\hat{H}_{\text{eff}} = \hat{H}_0 + \mathcal{O}(\frac{1}{\omega^2})$.

Within this setting (namely local driving with $\hat{V}^{(j)}$ and $\hat{V}^{(-j)}$ commuting), we have that to second order in $\frac{1}{\omega}$ the resources to simulate \hat{H}_{eff} are determined by the requirements for simulating \hat{H}_0 . This is one of the main benefits of the QHiFFS algorithm. Namely, it allows one to reuse previously developed time-independent techniques and lift them to a Floquet Hamiltonian simulation [28–34]. For example, if \hat{H}_0 is diagonal, or it can be analytically diagonalized, then one can simulate evolution under \hat{H}_{eff} , and correspondingly evolution under $\hat{H}(t)$, using a fixed depth circuit. The transversely driven Ising model (independent of topology and dimension) falls into this category. More generally, one could use known methods for simulating the time-independent 1D XY-model [28], Bethe diagonalizable models [71] and translationally symmetric models [34], to simulate the effect of local driving on such systems.

We note that in classical simulations of Floquet systems, high frequency expansions are known and commonly used [63, 65–68] both for simulation and for Floquet engineering. In the latter case, Eq. 3 and Eq. 4 are viewed from the opposite perspective to the one we take here. Namely, the time-dependent driving term, $\hat{V}(t)$, can be designed to implement otherwise unfeasible complex many-body time-independent Hamiltonians, \hat{H}_{eff} . This perspective is also taken in the quantum computing community for gate calibration and optimisation [72–74]. However, on digital quantum computers the harder task is typically to simulate the time-ordered integral. Hence, this is our focus here. Namely, we propose implementing Eq. (4) on quantum hardware to simulate Floquet dynamics.

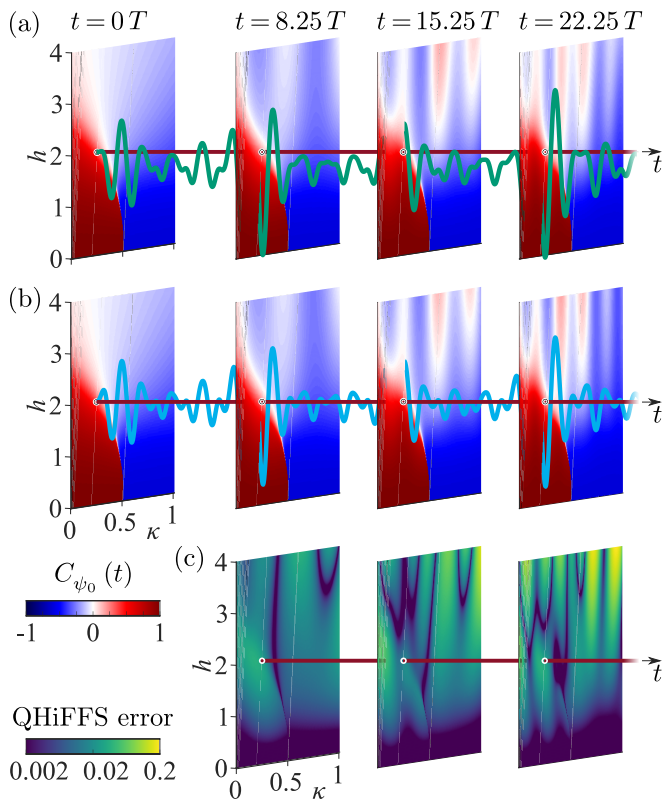


FIG. 2. **Numerical simulations of non-equilibrium dynamics of the transverse field BNNNI model.** Two-dimensional slices of the next-nearest-neighbor correlation function, $C_{\psi_0}(t)$, as a function of h and κ for different simulation times t computed exactly (a) and computed via 1st order QHiFFS (b). Here $J = 1$ and $\omega = 30$. The green/blue curves plot the exact/QHiFFS correlation function $C_{\psi_0}(t)$ as a function of time for the parameters $h = 2$ and $\kappa = 0.25$ also used in our hardware implementation (Fig. 3). In (c) we plot in logscale the error in the correlation function computed via QHiFFS - that is, the difference between the slices shown in (a) and (b). Videos corresponding to this figure can be found in the supplemental material.

III. Case study: Two-dimensional biaxial next-nearest-neighbor Ising (BNNNI) model in a transverse field

The transverse field BNNNI model is an example of an Ising model with next-nearest neighbor axial interactions [75–78]. Interest in such models is largely motivated by the following key facts: Firstly, the zero-temperature critical behavior of the quantum spin Ising system in D -dimensions is connected to the classical critical behavior of the corresponding $(D+1)$ -dimensional classical system. Secondly, the results of such systems can provide insight into the general role of quantum fluctuations in quantum magnetism and also have direct relevance to experiments on numerous frustrated quantum magnets [79] including CeSb [76], Ag₃Mg [77], Sn₂P₂S₆ [80], BaHo₂O₄ [81], SrDy₂O₄ [82]. While most work has focused on study-

ing non-driven models, the non-equilibrium quantum dynamics of one-dimensional models has also been explored in a quench protocol [78, 83].

Here we consider the two-dimensional Floquet driven transverse field BNNNI model [84] defined on a square lattice with the Hamiltonian

$$\hat{H}(t) = J \left(- \sum_{\langle i,j \rangle} \hat{Z}_i \hat{Z}_j + \kappa \sum_{\langle\langle i,j \rangle\rangle} \hat{Z}_i \hat{Z}_j \right) - h \cos(\omega t) \sum_i \hat{X}_i. \quad (8)$$

Here \hat{Z}, \hat{X} are Pauli operators, $\sum_{\langle i,j \rangle}$ denotes a sum over the nearest neighbors, and $\sum_{\langle\langle i,j \rangle\rangle}$ is a sum over axial next-nearest neighbors as shown in Fig. 1(b). For simplicity, below we consider only the case of $J, \kappa > 0$, for which the model is a paradigmatic example of frustrated magnetism.

Classical simulations of two-dimensional frustrated magnets are very challenging. Even their equilibrium properties are subject to long-standing controversy [85]. In general, classically simulating their non-equilibrium properties is even more challenging, which has stimulated widespread interest in their quantum simulation [86]. These challenges also limit our understanding of physics of the transverse field BNNNI model. Its static phase diagram is well-established for special cases. The zero-field ($h = 0$) system exhibits a phase transition from a ferromagnetic phase to an antiphase at $\kappa_c = \frac{1}{2}$ [84]. In the ferromagnetic phase, all spins point in the same direction, while in the antiphase one finds periodic sequences of 2 spins pointing in the same direction, followed by 2 spins pointing in the opposite direction [84]. The presence of a transverse magnetic field, $h\hat{X}$, introduces additional quantum fluctuations. For $\kappa = 0$, we recover the extensively studied transverse field quantum Ising model [87, 88] with ferromagnetic order for $h < h_c \approx 3.04$ [89]. At h_c the model undergoes a phase transition to a paramagnetic phase with all spins aligned in the \hat{X} direction.

To probe dynamical properties and nonequilibrium phases of this model we study the next-nearest-neighbor correlation function averaged over all qubits on the lattice. That is, for an $n_x \times n_y$ lattice, we compute

$$C_{\psi}(t) := \frac{1}{n_x n_y} \sum_{l_x=0}^{n_x-1} \sum_{l_y=0}^{n_y-1} \langle \psi | \hat{U}(t)^\dagger \hat{Z}_{l_x, l_y} \hat{Z}_{l_x, l_y+2} \hat{U}(t) | \psi \rangle \quad (9)$$

where $|\psi\rangle$ denotes an initial state of interest. To fit the lattice onto Quantinuum’s H1-1 quantum computer, in our hardware implementation, we consider a 4×5 lattice with periodic boundary conditions. The correlator $C_{\psi_0}(t) > 0$ indicates that directions of the next-nearest axial neighbor spins are aligned as in the ferromagnetic phase, while $C_{\psi_0}(t) < 0$ indicates that they are anti-aligned (as in the antiphase). This quantity can serve

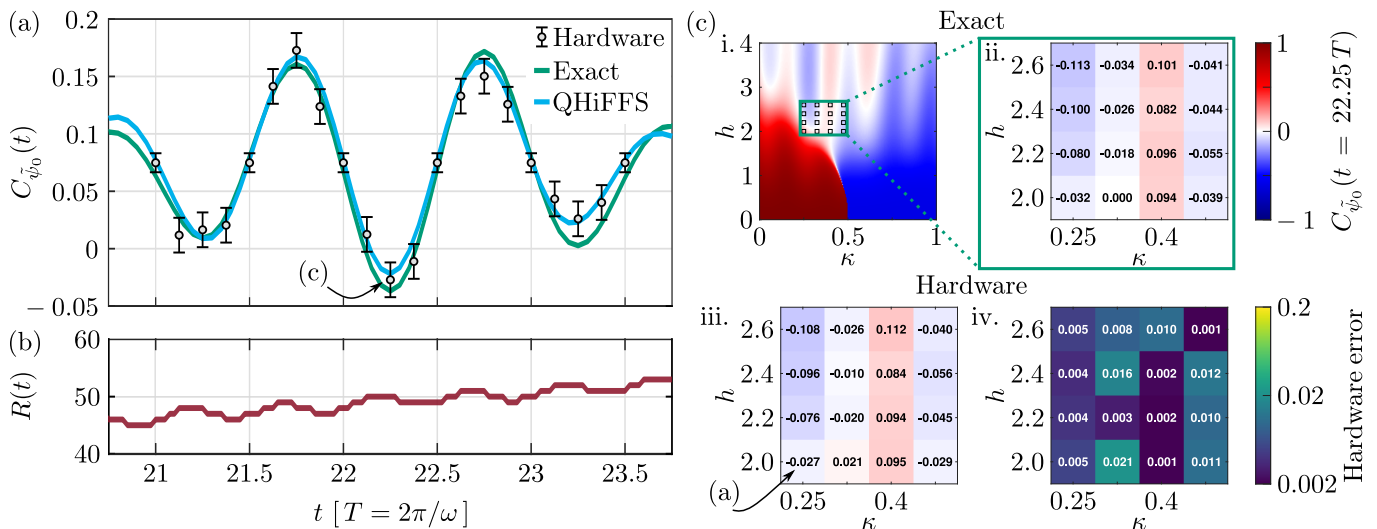


FIG. 3. **Hardware results:** (a) Here we plot $C_{\tilde{\psi}_0}(t)$, Eq. (9), the next-nearest-neighbor correlation function, for our short depth approximation of the ground (initial) state $|\tilde{\psi}_0\rangle$ averaged over all qubit sites k, l . The green line gives the exact correlation function value and the blue line is the correlation function as computed using the first order QHiFFS ansatz, which is implementable on quantum hardware by a shallow circuit (shown in Appendix A). The black data points are hardware results obtained from a 20-qubit Quantinuum H1-1 quantum computer. Their 2σ -error bars quantify uncertainty of the results due to finite shot number. (b) The red line compares the gate overhead required by Trotterization for the same (noise-free) algorithmic fidelity. That is, we plot $R(t) = N_{\text{Trotter}}(t)/N_{\text{QHiFFS}}(t)$ where $N_{\text{Trotter}}(t)$ ($N_{\text{QHiFFS}}(t)$) is the number of 2-qubit gates to simulate to time t with a second order Trotterization (the first order QHiFFS). To make $R(t)$ a fair comparison metric, the time step for the Trotterization is set to ensure the algorithmic error is the same for both methods. (c) Here we plot the $C_{\tilde{\psi}_0}(t)$ dependence on the parameters h and κ for a zoomed in region of the total parameter space (i.) at time $t = 22.25T$. (ii.) and (iii.) plot the exact correlation function values and those computed on quantum hardware respectively, with the error between them shown in (iv.).

to probe the field-induced phase change. In our case, we generally take $|\psi\rangle$ to be the ground state, denoted by $|\psi_0\rangle$ of $\hat{H}(t=0)$, setting $t_0 = 0$ in the following. The choice sets our simulations realistically connected with experimental situations. We stress that given the BNNNI model is translationally invariant, each term in the sum in Eq. (9) is identical and so $C_{\psi_0}(t)$ is equivalent to each of the individual qubit pair correlation functions. However, computing the average in Eq. (9) allows one to mitigate the effect of shot noise.

A. Numerical Simulations

We performed numerical simulations to study how well the QHiFFS algorithm captures short range correlation functions of the periodically driven BNNNI model. Figure 2(a) shows the next-nearest-neighbour correlation function, $C_{\psi_0}(t)$, as a function of h and κ for different simulation times. We chose $\omega = 30$, which ensures the applicability of the kick approximation for all considered parameter values of the model. Regions of ferromagnetic and antiferromagnetic correlation are indicated in red and blue respectively. We see that periodic driving further enriches the physics of the BNNNI model. In particular, when the BNNNI system is driven out of equilibrium by a high-frequency high-strength transverse field,

at long times a noticeable ferromagnetic instability can be induced out of an otherwise antiphase near the $\kappa = \frac{1}{2}$ quantum critical fan. This suggests that driven quantum systems are an exciting research area for generating and manipulating quantum phases.

Importantly, these complex changes are well-captured by the QHiFFS algorithm. This is shown in Fig. 2(b) where we plot the correlation function, $C_{\psi_0}(t)$, as computed using the QHiFFS algorithm. Indeed, as shown in Fig. 2(c), the errors in the correlation function (that is, the difference between the exact correlation function and the one computed via QHiFFS) are small. Specifically, the correlation function error on average (over the different h and κ values) is 0.0121 at $t = 8.25T$, 0.0175 at $t = 15.25T$ and 0.0216 at $t = 22.25T$.

B. Hardware Implementation

To demonstrate the suitability of the QHiFFS algorithm for real quantum hardware we used all 20 qubits of Quantinuum's H1-1 trapped ion platform to simulate the 4×5 BNNNI model with periodic boundary conditions (see Fig. 1). This was enabled by the all-to-all connectivity of the platform – on superconducting circuit devices (as compared to the trapped ion device that we used here), periodic boundary conditions on two-dimensional

lattice models are typically hard to implement due to the restriction to nearest-neighbor gates.

Due to a finite sampling budget of approximately 30,000 shots, we needed to restrict ourselves to specific model parameters. We decided to implement two studies - the first a simulation of the correlation function as a function of time, the second a slice of the correlation function at a fixed time plotted versus the model parameters. Without loss of generality, we took $J = 1$. For our plot of the correlation function as a function of time, we then chose $h = 2$, $\kappa = 0.25$, and $\omega = 30$ for which our numerical results indicate strong effects of periodic driving. For our study of model parameter dependence, we took $t = 22.25T$ and focused on the region $0.25 \leq \kappa \leq 0.475$ and $2.0 \leq h \leq 2.6$. The chosen parameters ensured that all model parameters are of a similar order of magnitude resulting in strong frustration and quantum fluctuations.

The first order QHiFFS ansatz yielded a constant depth circuit for Floquet time evolution, as both $\exp(-it\hat{H}_{\text{eff}})$ and $\exp(\pm i\hat{K}(t))$ were exactly implementable. Indeed, in the case of Quantinuum's H1-1 trapped ion device, with native single qubit rotations and two-qubit gates $\exp(-i\frac{\theta}{2}\hat{Z}\hat{Z})$, the simulation was implemented exactly with a fixed circuit using the native gate set. This meant that the QHiFFS circuit, for any simulation time, had the same depth as a single standard low-order Trotter-Suzuki step. Thus, the final simulation time t affected the error from the high-frequency approximation, but not the error from hardware imperfections.

Initial state preparation for a physically motivated quantum simulation is a non-trivial task, in general. In our case, preparing the ground states exactly would require deep circuits but using classical compilation techniques we found an approximation of the ground state that still captured the same underlying physics and required a much shorter depth circuit to prepare. Our final circuits used 40 2-qubit gates to prepare an approximation of the ground state for different h and κ with an average overlap of 0.964 relative to the true ground state. The complete quantum circuit for the full simulation consisted of 110 2-qubit gates and 120 single qubit gates (see Appendix A) for all non-half-integer time steps. At half-integer time steps the circuit implementing the time evolution compiled to the identity and so the circuit consisted of only the 40 gates required for state preparation.

In Fig. 3(a) we plot as a function of time: the correlation function obtained from our quantum hardware implementation (black data points), the exact value of the correlation function (green line) and the value predicted from classical simulations of the QHiFFS algorithm (blue line). Furthermore, for the hardware results we provide error bars quantifying their uncertainty due to a finite shot number as two standard deviations of the sample mean. Fig. 3(b) shows the ratio of the number of 2-qubit gates that would have been required for a Trotter simulation as compared to a QHiFFS simulation for the same average simulation fidelity. This varied from 45-fold (at short times) to 53-fold (at long times) and thus the

Trotter simulation was not feasible to be implemented on quantum hardware.

In Fig. 3(c) we plot the zoomed in $C_\psi(t)$ dependence on the parameters at time $t = 22.25T$ computed exactly and as computed on quantum hardware. The hardware error is less than 0.021 for all data points. Our implementation successfully captures the noticeable ferromagnetic instability induced out of the antiphase at the $\kappa = \frac{1}{2}$ quantum critical fan. This suggests that QHiFFS could open up new avenues to study novel driven quantum phases and criticality in strongly correlated electron systems. This could become particularly relevant experimentally when material systems with interesting high energy scales are subject to an electromagnetic field (e.g., light, high-harmonic generation).

The expected values of the correlation function are largely within our shot-noise based error bars, implying that our simulation (despite the considerable circuit depth and qubit number) is predominantly shot noise limited. Indeed, the simulation is also limited by the size of the available hardware - we chose to study a 20 qubit simulation not because this was the largest QHiFFS could handle, but rather because the Quantinuum H1-1 system was the largest all-to-all device to which we had access.

C. Error Analysis

To place the algorithm on solid conceptual foundations, as well as better understand the results of our numerical simulations and hardware implementations, we have conducted an analysis of QHiFFS algorithmic errors. To quantitatively judge the quality of a given Floquet simulation, we consider the average simulation infidelity over the uniform distribution of input states

$$\epsilon(\hat{U}_1, \hat{U}_2) := 1 - \mathbb{E} \left[\left| \langle \psi | \hat{U}_1^\dagger \hat{U}_2 | \psi \rangle \right|^2 \right]_{|\psi\rangle \sim \text{Haar}_n}. \quad (10)$$

Here we provide a summary of our error analysis for the transversely driven BNNNI model. In Appendix B, we frame our error analysis more generally.

We start by analysing the scaling of errors for the standard Trotterisation approach. As shown in detail in Appendix C, there are three sources of error in this case, one coming from the discretization of the time-ordered integral, one coming from the non-commutativity of the Hamiltonian at different times and another (the standard time-independent Trotter error) coming from the non-commutativity of terms in the Hamiltonian at a fixed time. The dominant contribution in the high-frequency regime comes from discretization, while the errors from non-commutativity are comparably small. We find that the average infidelity for the transverse BNNNI model scales as

$$\epsilon(\hat{U}_{\text{exact}}(t), \hat{U}_{\text{Trotter}}(t)) = \mathcal{O} \left(\frac{nh^2 t^4 \omega^2}{8m^2} \right). \quad (11)$$

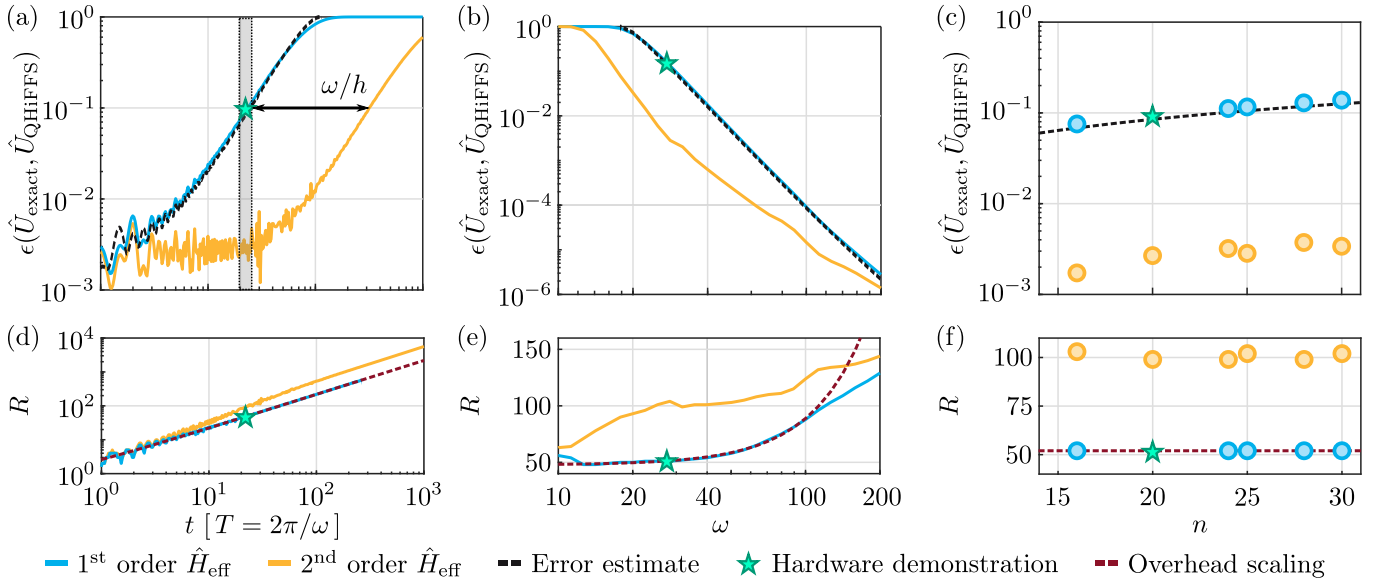


FIG. 4. **Error analysis.** Here we plot the average fidelity as a function of (a) simulation time t , (b) frequency ω and (c) system size n . Unless varied, the parameters equal those of our hardware implementation in Fig. 3; namely $J = 1$, $\kappa = 0.25$, $h = 2$, $\omega = 30$ and $t = 22.75T$. Overall, we find an excellent agreement between our analytical error estimate (black) and the exact numerical calculations (cyan). (Note, we plot here the full 1st-order expression for the error given in Eq. (12) in Appendix B). The yellow line indicates the exact error when \hat{H}_{eff} is expanded to second order in ω and the kick operator is expanded to first order in ω . (d), (e) and (f) show the numerically calculated overhead of standard Trotterization R in terms of simulation time t , frequency ω and system size n . For first order QHiFFS (cyan) we observe linear, quadratic (since t is chosen in units of $T = \frac{2\pi}{\omega}$) and constant scalings with t , ω and n respectively (shown in red) as predicted by Eq. (13).

where m is the number of Trotter steps and n is the system size. Thus, in contrast to standard time-independent Trotterization, the error here is independent of \hat{H}_0 and scales as t^4 rather than t^2 .

In comparison, we find that the long time error for the transversely driven BNNNI model when simulated by QHiFFS, scales as

$$\epsilon(\hat{U}_{\text{exact}}(t), \hat{U}_{\text{QHIFFS}}(t)) \approx \frac{281}{32} \frac{n \cdot h^4 \cdot (1 + \kappa^2) \cdot J^2 \cdot t^2}{\omega^4}. \quad (12)$$

The dominant contribution here is from the high-frequency truncation of the effective Hamiltonian. At short times, the truncation of the Kick approximation also contributes a significant oscillatory error to the averaged infidelity. However, the relative significance of this effect is washed out at longer times due to the contribution from the effective Hamiltonian which grows quadratically in time (compare Appendix B).

To support our analysis, we numerically computed the exact errors for the transversely driven BNNNI model. Specifically, in Fig. 4 we plot these errors, and our corresponding error estimates for the parameter regime we simulated on quantum hardware. Namely, a 4×5 two-dimensional transversely-driven BNNNI model with $J = 1$, $\kappa = 0.25$, $h = 2$, $\omega = 30$ (in (a)) and $t = 22.75T$ (in (b)). Overall, we find an excellent, nearly indistinguishable, agreement with our analysis.

Our error analysis further allows us to estimate how the

circuit depth of a standard Trotterization needs to scale compared to QHiFFS to achieve the same fidelity. Let R be the ratio of the number of two qubit gates used by Trotterization compared to the number of two qubit gates used by QHiFFS. For the driven BNNNI model presented here $R = m$, the number of Trotter steps used by the Trotterization since the 1st-order QHiFFS requires the same number of two qubit gates as one (1st- or 2nd-order) Trotter step. Specifically, using Eq. (11) and Eq. (12) we find that for the two-dimensional driven BNNNI model, R scales as

$$R = \mathcal{O}\left(\frac{t\omega^3}{Jh\sqrt{1+\kappa^2}}\right). \quad (13)$$

This scaling well-reproduces that computed numerically. Namely, the Trotter overhead grows linearly in time, as shown in Fig. 3(b) and Fig. 4(d), and cubically in ω , as shown in Fig. 4(e). We stress that this observation is independent of system size, n , as shown in Fig. 4(f).

The advantage of the QHiFFS ansatz can be further boosted by truncation at higher orders in k , (i.e. $(1/\omega)^k$). If we truncate at order k , the ratio of circuit depths becomes

$$R = \mathcal{O}\left(\frac{t\omega^2}{J\sqrt{1+\kappa^2}} \left(\frac{\omega}{h}\right)^k\right). \quad (14)$$

Such higher order expansions open up the simulation of longer times and larger system sizes without increasing

the algorithmic approximation infidelity, giving a significant advantage to the QHiFFS approach.

IV. Discussion

Here we have proposed the QHiFFS algorithm for simulating periodically driven systems on digital quantum computers. Central to the algorithm is the use of a kick operator to transform the problem into a frame of reference where the dynamics of the system is governed by a time-independent effective Hamiltonian. Thus, this method avoids the costly discretization of the time-ordered integral required by standard Trotterization and allows one to re-use previous time-independent Hamiltonian simulation methods [28–34]. In parallel, QHiFFS does not require any form of variational optimization of the sort required by many other near-term simulation methods [31–35, 37, 38, 90].

In special cases, namely those where the non-interacting Hamiltonian is diagonal and the driving term involves only a single local driving term, a fixed depth circuit can be used to simulate arbitrary times with an algorithmic error that grows quadratically in time. Thus, in this limit, the QHiFFS algorithm provides a new method for approximate *fast-forwarding* quantum simulations [31–33, 35, 91] that is highly suitable to near-term hardware. We stress that while the simulation in such cases is particularly simple, and thus also simpler to simulate classically, we still expect QHiFFS to be a useful stepping stone towards quantum advantage. This is because even the fixed depth circuits enabled by the kick approximation could be challenging to simulate classically. In general, apart from special cases like Clifford circuits or one-dimensional low entangled states [92, 93], the classical cost of simulating quantum circuits grows exponentially with circuit depth [94]. Therefore, one may expect that sufficiently deep and entangling fixed-depth QHiFFS circuits will be challenging to simulate classically in higher spatial dimensions. Given that these gate sequences are good approximations of the dynamics of quantum many-body systems that are forced out of equilibrium by a high frequency drive, such strong entanglement generation is a natural expectation.

Furthermore, even in the case where QHiFFS is classically simulable for some input states, it could still be used to implement classically intractable simulations for non-classically simulable initial states. Such states could plausibly be prepared via analogue simulation strategies. This could provide one of the earliest avenues for physically interesting non-classically simulable implementations of QHiFFS on near-term hardware.

However, QHiFFS is also much more broadly applicable and we expect the algorithm to find use in the fault-tolerant era as well as the near-term. In the latter case, one could use higher order expansions of the effective Hamiltonian and kick operators to achieve a higher accuracy, and implement the more complex resulting ef-

fective Hamiltonian using well-established fault-tolerant simulation methods [29, 30].

To benchmark QHiFFS we performed a 20-qubit simulation of the periodically driven two-dimensional BNNI model on Quantinuum’s 20-qubit H1-1 trapped ion platform. As shown in Fig. 3, the correlation function values computed on the quantum computer capture the true predicted values up to the precision allowed by shot noise ($2\sigma = 1.49 \cdot 10^{-2}$). In contrast, standard Trotterization (specifically a 2nd order Trotterization with the same algorithmic error as a 1st order QHiFFS) would have required approximately 50 times as many two-qubit gates, making the method completely unfeasible on current hardware due to gate errors and decoherence.

Our error scaling analysis demonstrates that QHiFFS outperforms standard Trotterization for high driving frequencies, ω . Specifically, at long simulation times, t , we see a linear advantage in t and at least cubic improvements in ω compared to standard Trotterization. In parallel, the algorithmic errors of QHiFFS scale linearly in system size, n , for local models, and at worst quadratically. These favourable scalings again point towards QHiFFS’s suitability for larger scale implementations.

Future interesting applications of QHiFFS on quantum hardware could include the simulation of strongly correlated systems in the presence of linearly or circularly polarized electromagnetic field for the study of the emergence of unconventional superconductivity [95], quantum spin liquids [96], and Kondo coherence collapse [97]. Similarly, one could study even more complicated, approximately fast-forwardable Ising models, either by adding longer range interactions or by studying three spatial dimensions. We believe the latter would be viable with current gate fidelities, e.g. on Quantinuum’s trapped ion device, but (for a non-trivial simulation) would require more qubits.

Acknowledgments

We thank Frédéric Sauvage and Martin Eckstein for helpful conversations. This work was supported by the Erlangen National High Performance Computing Center, the Quantum Science Center (QSC), a National Quantum Information Science Research Center of the U.S. Department of Energy (DOE), Los Alamos National Laboratory DOE ASCR and Munich Quantum Valley, which is supported by the Bavarian state government with funds from the Hightech Agenda Bayern Plus. This research used resources of the Oak Ridge Leadership Computing Facility, which is a DOE Office of Science User Facility supported under Contract DE-AC05-00OR22725. The research for this publication has been supported by a grant from the Priority Research Area DigiWorld under the Strategic Programme Excellence Initiative at Jagiellonian University. TE acknowledges support from the International Max-Planck Research

School for Physics of Light. PC acknowledges support by the National Science Centre (NCN), Poland under project 2019/35/B/ST3/01028. Work at Los Alamos was carried out under the auspices of the U.S. Department of Energy (DOE) National Nuclear Security Administration (NNSA) under Contract No. 89233218CNA000001, and was supported by the Laboratory Directed Research

and Development program of Los Alamos National Laboratory under project number 20220253ER (JXZ, ATS), as well as by 20230049DR (LC). ZH acknowledges initial support from the LANL Mark Kac Fellowship and subsequent support from the Sandoz Family Foundation-Monique de Meuron program for Academic Promotion.

-
- [1] Mark S Rudner, Netanel H Lindner, Erez Berg, and Michael Levin, “Anomalous edge states and the bulk-edge correspondence for periodically driven two-dimensional systems,” *Physical Review X* **3**, 031005 (2013).
- [2] Vedika Khemani, Achilleas Lazarides, Roderich Moessner, and Shivaji L Sondhi, “Phase structure of driven quantum systems,” *Physical review letters* **116**, 250401 (2016).
- [3] Roderich Moessner and Shivaji Lal Sondhi, “Equilibration and order in quantum Floquet matter,” *Nature Physics* **13**, 424–428 (2017).
- [4] Dominic V Else, Bela Bauer, and Chetan Nayak, “Prethermal phases of matter protected by time-translation symmetry,” *Physical Review X* **7**, 011026 (2017).
- [5] Ivar Martin, Gil Refael, and Bertrand Halperin, “Topological frequency conversion in strongly driven quantum systems,” *Physical Review X* **7**, 041008 (2017).
- [6] Roderich Moessner and Joel E. Moore, *Topological Phases of Matter* (Cambridge University Press, 2021).
- [7] Netanel H Lindner, Gil Refael, and Victor Galitski, “Floquet topological insulator in semiconductor quantum wells,” *Nature Physics* **7**, 490–495 (2011).
- [8] JH Mentink, Karsten Balzer, and Martin Eckstein, “Ultrafast and reversible control of the exchange interaction in mott insulators,” *Nature Communications* **6**, 6708 (2015).
- [9] Matteo Mitrano, Alice Cantaluppi, Daniele Nicoletti, Stefan Kaiser, A Perucchi, S Lupi, P Di Pietro, D Pontiroli, M Riccò, Stephen R Clark, *et al.*, “Possible light-induced superconductivity in K_3C_{60} at high temperature,” *Nature* **530**, 461–464 (2016).
- [10] DN Basov, RD Averitt, and D Hsieh, “Towards properties on demand in quantum materials,” *Nature materials* **16**, 1077–1088 (2017).
- [11] James W McIver, Benedikt Schulte, F-U Stein, Toru Matsuyama, Gregor Jotzu, Guido Meier, and Andrea Cavalleri, “Light-induced anomalous Hall effect in graphene,” *Nature physics* **16**, 38–41 (2020).
- [12] Frank Wilczek, “Quantum time crystals,” *Physical review letters* **109**, 160401 (2012).
- [13] Jiehang Zhang, Paul W Hess, A Kyprianidis, Petra Becker, A Lee, J Smith, Gaetano Pagano, I-D Potirniche, Andrew C Potter, Ashvin Vishwanath, *et al.*, “Observation of a discrete time crystal,” *Nature* **543**, 217–220 (2017).
- [14] Matteo Ippoliti, Kostyantyn Kechedzhi, Roderich Moessner, SL Sondhi, and Vedika Khemani, “Many-body physics in the NISQ era: quantum programming a discrete time crystal,” *PRX Quantum* **2**, 030346 (2021).
- [15] Xiao Mi, Matteo Ippoliti, Chris Quintana, Ami Greene, Zijun Chen, Jonathan Gross, Frank Arute, Kunal Arya, Juan Atalaya, Ryan Babbush, *et al.*, “Time-crystalline eigenstate order on a quantum processor,” *Nature* **601**, 531–536 (2022).
- [16] Philipp Frey and Stephan Rachel, “Realization of a discrete time crystal on 57 qubits of a quantum computer,” *Science advances* **8**, eabm7652 (2022).
- [17] J Randall, CE Bradley, FV van der Grienden, Asier Galicia, MH Abobeih, Matthew Markham, DJ Twitchen, Francisco Machado, NY Yao, and Tim Hugo Taminiau, “Many-body-localized discrete time crystal with a programmable spin-based quantum simulator,” *Science* **374**, 1474–1478 (2021).
- [18] Andrew C Potter, Takahiro Morimoto, and Ashvin Vishwanath, “Classification of interacting topological Floquet phases in one dimension,” *Physical Review X* **6**, 041001 (2016).
- [19] Philipp T Dumitrescu, Justin G Bohnet, John P Gaebler, Aaron Hankin, David Hayes, Ajesh Kumar, Brian Neyenhuis, Romain Vasseur, and Andrew C Potter, “Dynamical topological phase realized in a trapped-ion quantum simulator,” *Nature* **607**, 463–467 (2022).
- [20] Xu Zhang, Wenjie Jiang, Jinfeng Deng, Ke Wang, Jiachen Chen, Pengfei Zhang, Wenhui Ren, Hang Dong, Shibo Xu, Yu Gao, *et al.*, “Digital quantum simulation of Floquet symmetry-protected topological phases,” *Nature* **607**, 468–473 (2022).
- [21] Richard P. Feynman, “Simulating physics with computers,” *International Journal of Theoretical Physics* **21**, 467–488 (1982).
- [22] Norbert Schuch, Michael M Wolf, Frank Verstraete, and J Ignacio Cirac, “Entropy scaling and simulability by matrix product states,” *Physical Review Letters* **100**, 030504 (2008).
- [23] Michael M Wolf, “Violation of the entropic area law for fermions,” *Physical review letters* **96**, 010404 (2006).
- [24] Frank Arute, Kunal Arya, Ryan Babbush, Dave Bacon, Joseph C. Bardin, Rami Barends, Rupak Biswas, Sergio Boixo, Fernando G. S. L. Brandao, David A. Buell, Brian Burkett, Yu Chen, Zijun Chen, Ben Chiaro, Roberto Collins, William Courtney, Andrew Dunsworth, Edward Farhi, Brooks Foxen, Austin Fowler, Craig Gidney, Marissa Giustina, Rob Graff, Keith Guerler, Steve Habegger, Matthew P. Harrigan, Michael J. Hartmann, Alan Ho, Markus Hoffmann, Trent Huang, Travis S. Humble, Sergei V. Isakov, Evan Jeffrey, Zhang Jiang, Dvir Kafri, Kostyantyn Kechedzhi, Julian Kelly, Paul V. Klimov, Sergey Knysh, Alexander Korotkov, Fedor Kostritsa, David Landhuis, Mike Lindmark, Erik Lucero, Dmitry Lyakh, Salvatore Mandrà, Jarrod R. McClean, Matthew McEwen, Anthony Megrant, Xiao Mi, Kristel Michielsen, Masoud Mohseni, Josh Mutus, Ofer Naaman, Matthew Neeley, Charles Neill, Murphy Yuezhen Niu, Eric Os-

- ty, Andre Petukhov, John C. Platt, Chris Quintana, Eleanor G. Rieffel, Pedram Roushan, Nicholas C. Rubin, Daniel Sank, Kevin J. Satzinger, Vadim Smelyanskiy, Kevin J. Sung, Matthew D. Trevithick, Amit Vainsencher, Benjamin Villalonga, Theodore White, Z. Jamie Yao, Ping Yeh, Adam Zalcman, Hartmut Neven, and John M. Martinis, “Quantum supremacy using a programmable superconducting processor,” *Nature* **574**, 505–510 (2019).
- [25] Han-Sen Zhong, Hui Wang, Yu-Hao Deng, Ming-Cheng Chen, Li-Chao Peng, Yi-Han Luo, Jian Qin, Dian Wu, Xing Ding, Yi Hu, *et al.*, “Quantum computational advantage using photons,” *Science* **370**, 1460–1463 (2020).
- [26] Seth Lloyd, “Universal quantum simulators,” *Science*, 1073–1078 (1996).
- [27] AT Sornborger and Ewan D Stewart, “Higher-order methods for simulations on quantum computers,” *Physical Review A* **60**, 1956 (1999).
- [28] Frank Verstraete, J Ignacio Cirac, and José I Latorre, “Quantum circuits for strongly correlated quantum systems,” *Physical Review A* **79**, 032316 (2009).
- [29] Dominic W Berry, Andrew M Childs, Richard Cleve, Robin Kothari, and Rolando D Somma, “Simulating Hamiltonian dynamics with a truncated Taylor series,” *Physical Review Letters* **114**, 090502 (2015).
- [30] Guang Hao Low and Isaac L Chuang, “Hamiltonian simulation by qubitization,” *Quantum* **3**, 163 (2019).
- [31] Cristina Cirstoiu, Zoe Holmes, Joseph Iosue, Lukasz Cincio, Patrick J. Coles, and Andrew Sornborger, “Variational fast forwarding for quantum simulation beyond the coherence time,” *npj Quantum Information* **6**, 1–10 (2020).
- [32] Joe Gibbs, Kaitlin Gili, Zoë Holmes, Benjamin Commeau, Andrew Arrasmith, Lukasz Cincio, Patrick J. Coles, and Andrew Sornborger, “Long-time simulations with high fidelity on quantum hardware,” *arXiv preprint arXiv:2102.04313* (2021).
- [33] Joe Gibbs, Zoe Holmes, Matthias C. Caro, Nicholas Ezzell, Hsin-Yuan Huang, Lukasz Cincio, Andrew T. Sornborger, and Patrick J. Coles, “Dynamical simulation via quantum machine learning with provable generalization,” *arXiv preprint arXiv:2204.10269* (2022).
- [34] Refik Mansuroglu, Timo Eckstein, Ludwig Nützel, Samuel A Wilkinson, and Michael J Hartmann, “Variational Hamiltonian simulation for translational invariant systems via classical pre-processing,” *Quantum Science and Technology* (2021), <https://doi.org/10.1088/2058-9565/acb1d0>.
- [35] Efehan Kökcü, Thomas Steckmann, JK Freericks, Eugene F Dumitrescu, and Alexander F Kemper, “Fixed depth Hamiltonian simulation via Cartan decomposition,” *arXiv preprint arXiv:2104.00728* (2021).
- [36] Colin J Trout, Muyuan Li, Mauricio Gutiérrez, Yukai Wu, Sheng-Tao Wang, Luming Duan, and Kenneth R Brown, “Simulating the performance of a distance-3 surface code in a linear ion trap,” *New Journal of Physics* **20**, 043038 (2018).
- [37] Suguru Endo, Jinzhao Sun, Ying Li, Simon C Benjamin, and Xiao Yuan, “Variational quantum simulation of general processes,” *Physical Review Letters* **125**, 010501 (2020).
- [38] Yong-Xin Yao, Niladri Gomes, Feng Zhang, Cai-Zhuang Wang, Kai-Ming Ho, Thomas Iadecola, and Peter P Orth, “Adaptive variational quantum dynamics simulations,” *PRX Quantum* **2**, 030307 (2021).
- [39] Matthew Otten, Cristian L Cortes, and Stephen K Gray, “Noise-resilient quantum dynamics using symmetry-preserving ansatzes,” *arXiv preprint arXiv:1910.06284* (2019).
- [40] Marcello Benedetti, Mattia Fiorentini, and Michael Lubasch, “Hardware-efficient variational quantum algorithms for time evolution,” *arXiv preprint arXiv:2009.12361* (2020).
- [41] Stefano Barison, Filippo Vicentini, and Giuseppe Carleo, “An efficient quantum algorithm for the time evolution of parameterized circuits,” *arXiv preprint arXiv:2101.04579* (2021).
- [42] Kishor Bharti and Tobias Haug, “Quantum-assisted simulator,” *Physical Review A* **104**, 042418 (2021).
- [43] Jonathan Wei Zhong Lau, Kishor Bharti, Tobias Haug, and Leong Chuan Kwek, “Quantum assisted simulation of time dependent Hamiltonians,” *arXiv preprint arXiv:2101.07677* (2021).
- [44] Philipp-Immanuel Schneider and Alejandro Saenz, “Quantum computation with ultracold atoms in a driven optical lattice,” *Physical Review A* **85**, 050304 (2012).
- [45] Benedikt Fauseweh and Jian-Xin Zhu, “Digital quantum simulation of non-equilibrium quantum many-body systems,” *Quantum Information Processing* **20**, 1–16 (2021).
- [46] Benedikt Fauseweh and Jian-Xin Zhu, “Quantum computing Floquet band structures,” *arXiv preprint arXiv:2112.04276* (2021), <https://doi.org/10.48550/arXiv.2112.04276>.
- [47] Henry Lamm and Scott Lawrence, “Simulation of nonequilibrium dynamics on a quantum computer,” *Physical review letters* **121**, 170501 (2018).
- [48] Lindsay Bassman Oftelie, Kuang Liu, Aravind Krishnamoorthy, Thomas Linker, Yifan Geng, Daniel Shebib, Shogo Fukushima, Fuyuki Shimojo, Rajiv K Kalia, Aichiro Nakano, *et al.*, “Towards simulation of the dynamics of materials on quantum computers,” *Physical Review B* **101**, 184305 (2020).
- [49] Martin Rodriguez-Vega, Ella Carlander, Adrian Bahri, Ze-Xun Lin, Nikolai A Sinitsyn, and Gregory A Fiete, “Real-time simulation of light-driven spin chains on quantum computers,” *Physical Review Research* **4**, 013196 (2022).
- [50] Kaoru Mizuta and Keisuke Fujii, “Optimal time-periodic Hamiltonian simulation with Floquet-Hilbert space,” *arXiv preprint arXiv:2209.05048* (2022).
- [51] Jarrod R McClean, Sergio Boixo, Vadim N Smelyanskiy, Ryan Babbush, and Hartmut Neven, “Barren plateaus in quantum neural network training landscapes,” *Nature Communications* **9**, 1–6 (2018).
- [52] M. Cerezo, Akira Sone, Tyler Volkoff, Lukasz Cincio, and Patrick J Coles, “Cost function dependent barren plateaus in shallow parametrized quantum circuits,” *Nature Communications* **12**, 1–12 (2021).
- [53] Zoë Holmes, Kunal Sharma, M. Cerezo, and Patrick J Coles, “Connecting ansatz expressibility to gradient magnitudes and barren plateaus,” *PRX Quantum* **3**, 010313 (2022).
- [54] Zoë Holmes, Andrew Arrasmith, Bin Yan, Patrick J. Coles, Andreas Albrecht, and Andrew T Sornborger, “Barren plateaus preclude learning scramblers,” *Physical Review Letters* **126**, 190501 (2021).
- [55] Taylor L Patti, Khadijeh Najafi, Xun Gao, and Susanne F Yelin, “Entanglement devised barren plateau

- mitigation,” *Physical Review Research* **3**, 033090 (2021).
- [56] Carlos Ortiz Marrero, Mária Kieferová, and Nathan Wiebe, “Entanglement-induced barren plateaus,” *PRX Quantum* **2**, 040316 (2021).
- [57] Andrew Arrasmith, Zoë Holmes, Marco Cerezo, and Patrick J Coles, “Equivalence of quantum barren plateaus to cost concentration and narrow gorges,” *Quantum Science and Technology* **7**, 045015 (2022).
- [58] Samson Wang, Enrico Fontana, M. Cerezo, Kunal Sharma, Akira Sone, Lukasz Cincio, and Patrick J Coles, “Noise-induced barren plateaus in variational quantum algorithms,” *Nature Communications* **12**, 1–11 (2021).
- [59] Lennart Bittel and Martin Kliesch, “Training variational quantum algorithms is NP-hard,” *Phys. Rev. Lett.* **127**, 120502 (2021).
- [60] Javier Rivera-Dean, Patrick Huembeli, Antonio Acín, and Joseph Bowles, “Avoiding local minima in variational quantum algorithms with neural networks,” *arXiv preprint arXiv:2104.02955* (2021).
- [61] Eric R Anschuetz and Bobak T Kiani, “Beyond barren plateaus: Quantum variational algorithms are swamped with traps,” *arXiv preprint arXiv:2205.05786* (2022).
- [62] Gaston Floquet, “Sur les équations différentielles linéaires à coefficients périodiques,” *Ann. cole Norm. Sup* **12**, 4788 (1883).
- [63] Wilhelm Magnus, “On the exponential solution of differential equations for a linear operator,” *Communications on pure and applied mathematics* **7**, 649–673 (1954).
- [64] Jon H Shirley, “Solution of the Schrödinger equation with a Hamiltonian periodic in time,” *Physical Review* **138**, B979 (1965).
- [65] Nathan Goldman and Jean Dalibard, “Periodically driven quantum systems: effective Hamiltonians and engineered gauge fields,” *Physical review X* **4**, 031027 (2014).
- [66] André Eckardt and Egidijus Anisimovas, “High-frequency approximation for periodically driven quantum systems from a Floquet-space perspective,” *New journal of physics* **17**, 093039 (2015).
- [67] Marin Bukov, Luca D’Alessio, and Anatoli Polkovnikov, “Universal high-frequency behavior of periodically driven systems: from dynamical stabilization to Floquet engineering,” *Advances in Physics* **64**, 139–226 (2015).
- [68] Takashi Oka and Sota Kitamura, “Floquet engineering of quantum materials,” *Annual Review of Condensed Matter Physics* **10**, 387–408 (2019).
- [69] KB Whaley and JC Light, “Rotating-frame transformations: A new approximation for multiphoton absorption and dissociation in laser fields,” *Physical Review A* **29**, 1188 (1984).
- [70] Saar Rahav, Ido Gilary, and Shmuel Fishman, “Effective Hamiltonians for periodically driven systems,” *Physical Review A* **68**, 013820 (2003).
- [71] Alejandro Sopena, Max Hunter Gordon, Diego García-Martín, Germán Sierra, and Esperanza López, “Algebraic Bethe Circuits,” *Quantum* **6**, 796 (2022).
- [72] Mahdi Sameti and Michael J Hartmann, “Floquet engineering in superconducting circuits: From arbitrary spin-spin interactions to the Kitaev honeycomb model,” *Physical Review A* **99**, 012333 (2019).
- [73] Francesco Petiziol, Mahdi Sameti, Stefano Carretta, Sandro Wimberger, and Florian Mintert, “Quantum simulation of three-body interactions in weakly driven quantum systems,” *Physical Review Letters* **126**, 250504 (2021).
- [74] Haifeng Qiao, Yadav P Kandel, John S Van Dyke, Saeed Fallahi, Geoffrey C Gardner, Michael J Manfra, Edwin Barnes, and John M Nichol, “Floquet-enhanced spin swaps,” *Nature Communications* **12**, 2142 (2021).
- [75] R Jo Elliott, “Phenomenological discussion of magnetic ordering in the heavy rare-earth metals,” *Physical Review* **124**, 346 (1961).
- [76] Per Bak and J. von Boehm, “Ising model with solitons, phasons, and “the devil’s staircase”,” *Phys. Rev. B* **21**, 5297–5308 (1980).
- [77] Walter Selke, “The ANNNI model—theoretical analysis and experimental application,” *Physics Reports* **170**, 213–264 (1988).
- [78] Vincenzo Alba and Maurizio Fagotti, “Prethermalization at low temperature: The scent of long-range order,” *Phys. Rev. Lett.* **119**, 010601 (2017).
- [79] Ivan Nekrashevich, Xiaxin Ding, Fedor Balakirev, Hee Taek Yi, Sang-Wook Cheong, Leonardo Civale, Yoshitomo Kamiya, and Vivien S. Zapf, “Reaching the equilibrium state of the frustrated triangular Ising magnet $\text{Ca}_3\text{Co}_2\text{O}_6$,” *Physical Review B* **105**, 024426 (2022).
- [80] V. Liubachko, A. Oleaga, A. Salazar, R. Yevych, A. Kohutych, and Yu. Vysochanskii, “Phase diagram of ferroelectrics with tricritical and Lifshitz points at coupling between polar and antipolar fluctuations,” *Phys. Rev. B* **101**, 224110 (2020).
- [81] Bobby Prévost, Nicolas Gauthier, Vladimir Y. Pomjakushin, Bernard Delley, Helen C. Walker, Michel Kenzelmann, and Andrea D. Bianchi, “Coexistence of magnetic fluctuations and long-range order in the one-dimensional J_1 – J_2 zigzag chain materials BaDy_2O_4 and BaHo_2O_4 ,” *Phys. Rev. B* **98**, 144428 (2018).
- [82] N. Gauthier, A. Fennell, B. Prévost, A. Désilets-Benoit, H. A. Dabkowska, O. Zaharko, M. Frontzek, R. Sibille, A. D. Bianchi, and M. Kenzelmann, “Field dependence of the magnetic correlations of the frustrated magnet SrDy_2O_4 ,” *Phys. Rev. B* **95**, 184436 (2017).
- [83] D. M. Kennes, D. Schuricht, and C. Karrasch, “Controlling dynamical quantum phase transitions,” *Phys. Rev. B* **97**, 184302 (2018).
- [84] R. M. Hornreich, R. Liebmann, H. G. Schuster, and W. Selke, “Lifshitz points in Ising systems,” *Zeitschrift für Physik B Condensed Matter* **35**, 91–97 (1979).
- [85] Lucile Savary and Leon Balents, “Quantum spin liquids: a review,” *Reports on Progress in Physics* **80**, 016502 (2016).
- [86] J. Eisert, M. Friesdorf, and C. Gogolin, “Quantum many-body systems out of equilibrium,” *Nature Physics* **11**, 124–130 (2015).
- [87] Pierre Pfeuty, “The one-dimensional Ising model with a transverse field,” *ANNALS of Physics* **57**, 79–90 (1970).
- [88] P Pfeuty and RJ Elliott, “The Ising model with a transverse field. II. ground state properties,” *Journal of Physics C: Solid State Physics* **4**, 2370 (1971).
- [89] Henk W. J. Blöte and Youjin Deng, “Cluster monte carlo simulation of the transverse Ising model,” *Phys. Rev. E* **66**, 066110 (2002).
- [90] Andi Gu, Angus Lowe, Pavel A Dub, Patrick J. Coles, and Andrew Arrasmith, “Adaptive shot allocation for fast convergence in variational quantum algorithms,” *arXiv preprint arXiv:2108.10434* (2021).
- [91] Shouzhen Gu, Rolando D. Somma, and Burak Şahinoğlu, “Fast-forwarding quantum evolution,” *Quantum* **5**, 577 (2021).
- [92] M. Fannes, B. Nachtergaele, and R. Werner, “Finitely

- correlated states on quantum spin chains,” *Comm. in Math. Phys.* **144**, 443–490 (1992).
- [93] Frank Verstraete, Valentin Murg, and J Ignacio Cirac, “Matrix product states, projected entangled pair states, and variational renormalization group methods for quantum spin systems,” *Advances in physics* **57**, 143–224 (2008).
- [94] Yong Liu, Xin Liu, Fang Li, Haohuan Fu, Yuling Yang, Jiawei Song, Pengpeng Zhao, Zhen Wang, Dajia Peng, Huarong Chen, Chu Guo, Heliang Huang, Wenzhao Wu, and Dexun Chen, “Closing the “quantum supremacy” gap: Achieving real-time simulation of a random quantum circuit using a new sunway supercomputer,” in *Proceedings of the International Conference for High Performance Computing, Networking, Storage and Analysis*, SC ’21 (Association for Computing Machinery, New York, NY, USA, 2021).
- [95] Umesh Kumar and Shi-Zeng Lin, “Inducing and controlling superconductivity in the Hubbard honeycomb model using an electromagnetic drive,” *Physical Review B* **103**, 064508 (2021).
- [96] Martin Claassen, Hong-Chen Jiang, Brian Moritz, and Thomas P Devereaux, “Dynamical time-reversal symmetry breaking and photo-induced chiral spin liquids in frustrated mott insulators,” *Nature Communications* **8**, 1192 (2017).
- [97] Wei Zhu, Benedikt Fauseweh, Alexis Chacon, and Jian-Xin Zhu, “Ultrafast laser-driven many-body dynamics and Kondo coherence collapse,” *Physical Review B* **103**, 224305 (2021).
- [98] “The Power of Block-Encoded Matrix Powers: Improved Regression Techniques via Faster Hamiltonian Simulation,” *46th International Colloquium on Automata, Languages, and Programming (ICALP 2019)*, *Leibniz International Proceedings in Informatics (LIPIcs)*, **132**, 33:1–33:14 (2019).

Supplementary Material for
 “Large-scale simulations of Floquet physics on near-term quantum computers”

A. Hardware quantum circuit

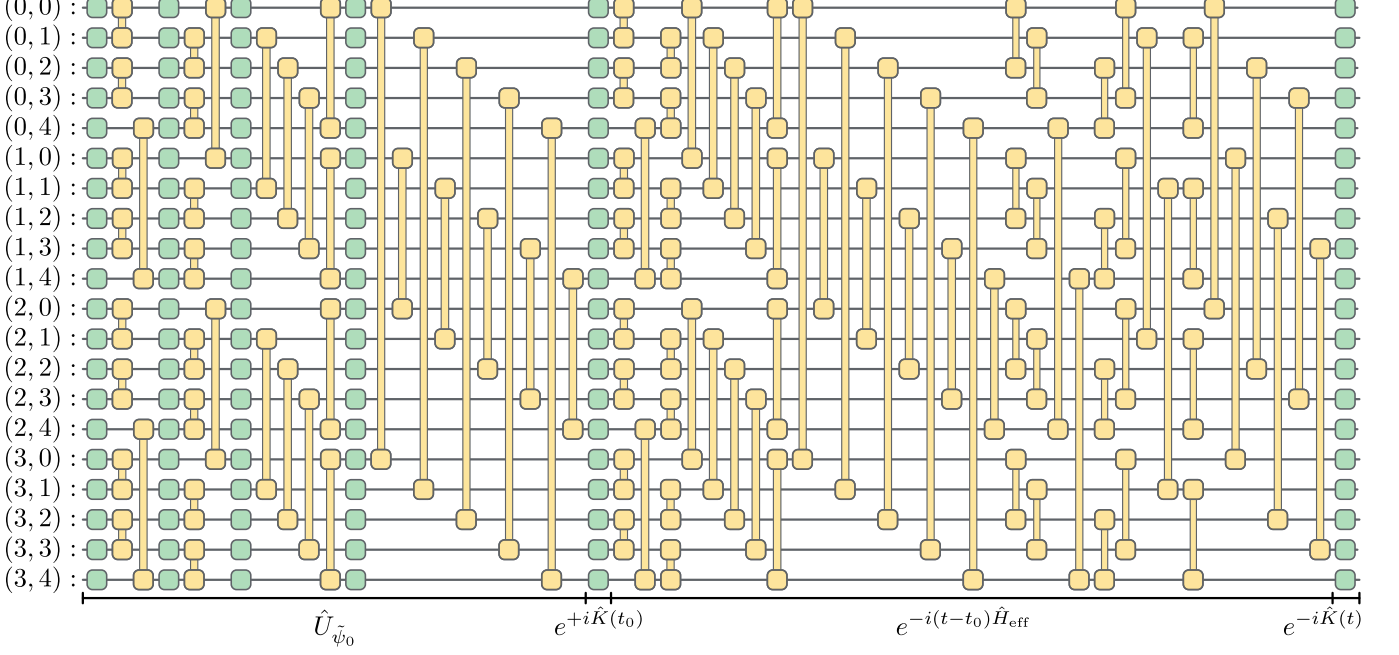


FIG. 5. **Quantum hardware circuit:** One-qubit gates are colored in green and two-qubit gates are depicted in yellow. The first 4 two-qubit layers (40 gates) are used for approximate preparation of the BNNNI model ground-state $|\psi_0\rangle$ (average overlap $\approx 96.4\%$). The remaining 7 two-qubit layers (70 gates) are used to implement $\exp(-i(t-t_0)\hat{H}_{\text{eff}}) \approx \exp(-i(t-t_0)\hat{H}_0)$. Both $\hat{K}(t)$ and \hat{H}_0 can be implemented exactly up to $\mathcal{O}(\frac{1}{\omega^2})$, which allows for constant depth approximate fast-forwarding.

B. QHiFFS Error Analysis

1. Derivation of kick operator and effective Hamiltonian

In this subsection we provide a detailed derivation of the effective Hamiltonian and kick operator for pedagogical purposes. This derivation was originally performed in Ref. [65].

We start with a periodic, time-dependent Hamiltonian,

$$\hat{H}(t) = \hat{H}_0 + \hat{V}(t), \quad \hat{V}(t) = \hat{V}(t+T). \quad (\text{B1})$$

Our aim is to transform to a basis in which the time evolution is generated by an effective, time-independent Hamiltonian, \hat{H}_{eff} ,

$$i\partial_t |\psi\rangle = \hat{H}(t) |\psi\rangle \implies i\partial_t |\phi\rangle = \hat{H}_{\text{eff}} |\phi(t)\rangle \quad \text{for } |\phi(t)\rangle = e^{i\hat{K}(t)} |\psi\rangle. \quad (\text{B2})$$

The so-called kick operator \hat{K} generates the basis change. Inserting the definition of $|\phi\rangle$ into the Schrödinger equation (Eq. (B2)) gives a defining relation for the effective Hamiltonian

$$\hat{H}_{\text{eff}} = e^{i\hat{K}(t)} \hat{H}(t) e^{-i\hat{K}(t)} + i \left(\frac{\partial e^{i\hat{K}(t)}}{\partial t} \right) e^{-i\hat{K}(t)}. \quad (\text{B3})$$

While Eq. (B3) is hard to solve in general, consistent perturbative expansions of the kick operator, $\hat{K}(t)$, and effective Hamiltonian, \hat{H}_{eff} , can be found in the high frequency regime. To do this, we expand in polynomial orders of the period, $\frac{T}{2\pi} = \frac{1}{\omega}$,

$$\hat{H}_{\text{eff}} = \sum_{k=0}^{\infty} \frac{\hat{H}_{\text{eff}}^{(k)}}{\omega^k}, \quad \hat{K}(t) = \sum_{k=1}^{\infty} \frac{\hat{K}^{(k)}(t)}{\omega^k}. \quad (\text{B4})$$

Note that the kick operator is periodic with the same period, T , as the potential, $V(t)$, which can be seen from Eq. (B3). We assume that the kick operator does not admit a constant 0^{th} order as it can be absorbed in H_0 without loss of generality. The first term on the right hand side of Eq. (B3) can be expanded using the Hadamard lemma, i.e. we have

$$e^{i\hat{K}(t)} \hat{H}(t) e^{-i\hat{K}(t)} = \sum_{q=0}^{\infty} \frac{i^q}{q!} \left[\hat{K}(t)_{(q)}, \hat{H}(t) \right], \quad (\text{B5})$$

where we denote q -fold nested commutators by $\left[\hat{K}(t)_{(q)}, \hat{H}(t) \right] = \left[\hat{K}(t), \left[\hat{K}(t)_{(q-1)}, \hat{H}(t) \right] \right]$. The second term can then be expanded using the well-known identity $\frac{\partial}{\partial x} e^{\hat{A}(x)} = \int_0^1 e^{y\hat{A}(x)} \left(\frac{\partial}{\partial x} \hat{A}(x) \right) e^{(1-y)\hat{A}(x)} dy$ and the Hadamard lemma, to give

$$i \left(\frac{\partial e^{i\hat{K}(t)}}{\partial t} \right) e^{-i\hat{K}(t)} = - \int_0^1 e^{ix\hat{K}(t)} \left(\frac{\partial}{\partial t} \hat{K}(t) \right) e^{-ix\hat{K}(t)} dx = - \sum_{q=0}^{\infty} \frac{i^q}{(q+1)!} \left[\hat{K}(t)_{(q)}, \frac{\partial \hat{K}(t)}{\partial t} \right]. \quad (\text{B6})$$

Finally, we use a Fourier decomposition of the potential $\hat{V}(t) = \sum_{j=1}^{\infty} \hat{V}^{(j)} e^{ij\omega t} + \hat{V}^{(-j)} e^{-ij\omega t}$ to show its frequency dependence. Note that hermiticity of $\hat{V}(t)$ implies $\hat{V}^{(j)\dagger} = \hat{V}^{(-j)}$. An order-by-order solution for $\hat{K}(t)$ and \hat{H}_{eff} can then be systematically achieved. For the k^{th} order, the steps are thus,

1. Write down k^{th} order of Eq. (B3).
2. Plug in all orders up to $k-1$ for \hat{H}_{eff} and k for $\hat{K}(t)$.
3. Define $\hat{K}^{(k+1)}(t)$ such that the right hand side of Eq. (B3) is time independent.
4. Read off $\hat{H}_{\text{eff}}^{(k)}$.

We demonstrate the method to find $\hat{K}(t)$ and \hat{H}_{eff} up to second order. The terms contributing to 0^{th} order in Eq. (B3) are

$$\hat{H}_{\text{eff}}^{(0)} = \hat{H}(t) - \frac{1}{\omega} \frac{\partial \hat{K}^{(1)}(t)}{\partial t} = \hat{H}_0 + \sum_{j=1}^{\infty} \left(\hat{V}^{(j)} e^{ij\omega t} + \hat{V}^{(-j)} e^{-ij\omega t} \right) - \frac{1}{\omega} \frac{\partial \hat{K}^{(1)}(t)}{\partial t}. \quad (\text{B7})$$

Although $K^{(1)}$ comes with a first order factor $\frac{1}{\omega}$, the term involving the time derivative $\frac{\partial}{\partial t} K^{(1)} = \mathcal{O}(\omega)$ is of 0^{th} order. This is because of the periodicity of $K(t)$ and can be straight-forwardly shown using the fact that the lowest frequency in its Fourier transform has to be ω . To eliminate the time-dependence in Eq. (B7), we define

$$\hat{K}^{(1)}(t) = -i \sum_{j=1}^{\infty} \frac{1}{j} \left(\hat{V}^{(j)} e^{ij\omega t} - \hat{V}^{(-j)} e^{-ij\omega t} \right), \quad (\text{B8})$$

which leaves us with $\hat{H}_{\text{eff}}^{(0)} = \hat{H}_0$. Next, to first order

$$\frac{1}{\omega} \hat{H}_{\text{eff}}^{(1)} = \frac{i}{\omega} \left[\hat{K}^{(1)}, \hat{H}(t) \right] - \frac{i}{2\omega^2} \left[\hat{K}^{(1)}, \frac{\partial \hat{K}^{(1)}(t)}{\partial t} \right] - \frac{1}{\omega^2} \frac{\partial \hat{K}^{(2)}(t)}{\partial t} \quad (\text{B9})$$

$$\begin{aligned} \iff \hat{H}_{\text{eff}}^{(1)} &= \sum_{j=1}^{\infty} \frac{1}{j} \left(\left[\hat{V}^{(j)}, \hat{H}_0 \right] e^{ij\omega t} + H.c. \right) + \frac{1}{2} \sum_{j,k=1}^{\infty} \frac{1}{j} \left(\left[\hat{V}^{(j)}, \hat{V}^{(k)} \right] e^{i(j+k)\omega t} + H.c. \right) \\ &+ \frac{1}{2} \sum_{j,k=1}^{\infty} \frac{1}{j} \left(\left[\hat{V}^{(j)}, \hat{V}^{(-k)} \right] e^{i(j-k)\omega t} + H.c. \right) - \frac{1}{\omega} \frac{\partial \hat{K}^{(2)}(t)}{\partial t}. \end{aligned} \quad (\text{B10})$$

Again, we identify the time-dependent terms and integrate them to fix

$$\begin{aligned} \hat{K}^{(2)}(t) = & -i \sum_{j=1}^{\infty} \frac{1}{j^2} \left([\hat{V}^{(j)}, \hat{H}_0] e^{ij\omega t} - H.c. \right) - \frac{i}{2} \sum_{j,k=1}^{\infty} \frac{1}{j(j+k)} \left([\hat{V}^{(j)}, \hat{V}^{(k)}] e^{i(j+k)\omega t} - H.c. \right) \\ & - \frac{i}{2} \sum_{j \neq k=1}^{\infty} \frac{1}{j(j-k)} \left([\hat{V}^{(j)}, \hat{V}^{(-k)}] e^{i(j-k)\omega t} - H.c. \right). \end{aligned} \quad (\text{B11})$$

and read off $\hat{H}_{\text{eff}}^{(1)} = \sum_{j=1}^{\infty} \frac{1}{j} [\hat{V}^{(j)}, \hat{V}^{(-j)}]$. Finally, we calculate \hat{H}_{eff} to second order,

$$\begin{aligned} \frac{1}{\omega^2} \hat{H}_{\text{eff}}^{(2)} = & \frac{i}{\omega^2} [\hat{K}^{(2)}, \hat{H}(t)] - \frac{1}{2\omega^2} [\hat{K}^{(1)}, [\hat{K}^{(1)}, \hat{H}(t)]] + \frac{1}{6\omega^3} \left[\hat{K}^{(1)}, \left[\hat{K}^{(1)}, \frac{\partial \hat{K}^{(1)}(t)}{\partial t} \right] \right] \\ & - \frac{i}{2\omega^3} \left[\hat{K}^{(1)}, \frac{\partial \hat{K}^{(2)}(t)}{\partial t} \right] - \frac{i}{2\omega^3} \left[\hat{K}^{(2)}, \frac{\partial \hat{K}^{(1)}(t)}{\partial t} \right] - \frac{1}{\omega^3} \frac{\partial \hat{K}^{(3)}(t)}{\partial t}. \end{aligned} \quad (\text{B12})$$

We can simplify this expression by first plugging in $\frac{\partial \hat{K}^{(1)}}{\partial t} = \omega \hat{V}(t)$.

$$\begin{aligned} \hat{H}_{\text{eff}}^{(2)} = & i [\hat{K}^{(2)}, \hat{H}_0] + \frac{i}{2} [\hat{K}^{(2)}, \hat{V}(t)] - \frac{1}{2} [\hat{K}^{(1)}, [\hat{K}^{(1)}, \hat{H}_0]] - \frac{1}{3} [\hat{K}^{(1)}, [\hat{K}^{(1)}, \hat{V}(t)]] \\ & - \frac{i}{2\omega} \left[\hat{K}^{(1)}, \frac{\partial \hat{K}^{(2)}(t)}{\partial t} \right] - \frac{1}{\omega} \frac{\partial \hat{K}^{(3)}(t)}{\partial t} \end{aligned} \quad (\text{B13})$$

We are more interested in $\hat{H}_{\text{eff}}^{(2)}$ than in $\hat{K}^{(3)}$, so we drop all time-dependent terms to find,

$$\begin{aligned} \hat{H}_{\text{eff}}^{(2)} = & \frac{1}{2} \sum_{j=1}^{\infty} \frac{1}{j^2} \left([[\hat{V}^{(j)}, \hat{H}_0], \hat{V}^{(-j)}] + H.c. \right) + \frac{1}{4} \sum_{j,k=1}^{\infty} \frac{1}{j(j+k)} \left([[\hat{V}^{(j)}, \hat{V}^{(k)}], \hat{V}^{(-j-k)}] + H.c. \right) \\ & + \frac{1}{4} \sum_{j \neq k=1}^{\infty} \frac{1}{j(j-k)} \left([[\hat{V}^{(j)}, \hat{V}^{(-k)}], \hat{V}^{(k-j)}] + H.c. \right) - \frac{1}{2} \sum_{j=1}^{\infty} \frac{1}{j^2} \left([\hat{V}^{(j)}, [\hat{V}^{(-j)}, \hat{H}_0]] + H.c. \right) \\ & + \frac{1}{3} \sum_{j,k=1}^{\infty} \frac{1}{jk} \left([\hat{V}^{(j)}, [\hat{V}^{(k)}, \hat{V}^{(-j-k)}]] + H.c. \right) - \frac{1}{3} \sum_{j \neq k=1}^{\infty} \frac{1}{jk} \left([\hat{V}^{(j)}, [\hat{V}^{(-k)}, \hat{V}^{(k-j)}]] + H.c. \right) \\ & + \frac{1}{2} \sum_{j=1}^{\infty} \frac{1}{j^2} \left([\hat{V}^{(-j)}, [\hat{V}^{(j)}, \hat{H}_0]] + H.c. \right) + \frac{1}{4} \sum_{j,k=1}^{\infty} \frac{1}{j(j+k)} \left([\hat{V}^{(-j-k)}, [\hat{V}^{(j)}, \hat{V}^{(k)}]] + H.c. \right) \\ & + \frac{1}{4} \sum_{j \neq k=1}^{\infty} \frac{1}{j(j-k)} \left([\hat{V}^{(k-j)}, [\hat{V}^{(j)}, \hat{V}^{(-k)}]] + H.c. \right) \end{aligned} \quad (\text{B14})$$

$$\begin{aligned} = & -\frac{1}{2} \sum_{j=1}^{\infty} \frac{1}{j^2} \left([\hat{V}^{(j)}, [\hat{V}^{(-j)}, \hat{H}_0]] + H.c. \right) + \frac{1}{3} \sum_{j,k=1}^{\infty} \frac{1}{jk} \left([\hat{V}^{(j)}, [\hat{V}^{(k)}, \hat{V}^{(-j-k)}]] + H.c. \right) \\ & - \frac{1}{3} \sum_{j \neq k=1}^{\infty} \frac{1}{jk} \left([\hat{V}^{(j)}, [\hat{V}^{(-k)}, \hat{V}^{(k-j)}]] + H.c. \right), \end{aligned} \quad (\text{B15})$$

which has contributions from all terms of Eq. (B13) except $i [\hat{K}^{(2)}, \hat{H}_0]$ and $-\frac{1}{\omega} \frac{\partial \hat{K}^{(3)}(t)}{\partial t}$, which do not include

time-independent terms. Putting together all terms up to second order, we find,

$$\begin{aligned} \hat{H}_{\text{eff}} = & \hat{H}_0 + \frac{1}{\omega} \sum_{j=1}^{\infty} \frac{1}{j} \left[\hat{V}^{(j)}, \hat{V}^{(-j)} \right] - \frac{1}{2\omega^2} \sum_{j=1}^{\infty} \frac{1}{j^2} \left(\left[\hat{V}^{(j)}, \left[\hat{V}^{(-j)}, \hat{H}_0 \right] \right] + H.c. \right) \\ & + \frac{1}{3} \sum_{j,k=1}^{\infty} \frac{1}{jk} \left(\left[\hat{V}^{(j)}, \left[\hat{V}^{(k)}, \hat{V}^{(-j-k)} \right] \right] + H.c. \right) - \frac{1}{3} \sum_{j \neq k=1}^{\infty} \frac{1}{jk} \left(\left[\hat{V}^{(j)}, \left[\hat{V}^{(-k)}, \hat{V}^{(k-j)} \right] \right] + H.c. \right) + \mathcal{O} \left(\frac{1}{\omega^3} \right), \end{aligned} \quad (\text{B16})$$

$$\begin{aligned} \hat{K}(t) = & -\frac{i}{\omega} \sum_{j=1}^{\infty} \frac{1}{j} \left(\hat{V}^{(j)} e^{ij\omega t} - \hat{V}^{(-j)} e^{-ij\omega t} \right) - \frac{i}{\omega^2} \sum_{j=1}^{\infty} \frac{1}{j^2} \left(\left[\hat{V}^{(j)}, \hat{H}_0 \right] e^{ij\omega t} - H.c. \right) \\ & - \frac{i}{2\omega^2} \sum_{j,k=1}^{\infty} \frac{1}{j(j+k)} \left(\left[\hat{V}^{(j)}, \hat{V}^{(k)} \right] e^{i(j+k)\omega t} - H.c. \right) \\ & - \frac{i}{2\omega^2} \sum_{j \neq k=1}^{\infty} \frac{1}{j(j-k)} \left(\left[\hat{V}^{(j)}, \hat{V}^{(-k)} \right] e^{i(j-k)\omega t} - H.c. \right) + \mathcal{O} \left(\frac{1}{\omega^3} \right) \end{aligned} \quad (\text{B17})$$

It becomes apparent from the above derivation that all orders of $\hat{K}(t)$ and \hat{H}_{eff} consist of commutator terms. Also note that in this work, the Fourier components of the driving potential commute, which further simplifies the high frequency expansion.

2. Special cases

Table I lists different special cases that can simplify expressions for \hat{H}_{eff} and $\hat{K}(t)$. We discuss the four classes of periodic systems in the following. Starting with the expressions (B16, B17) derived above, assume the periodic potential only admits a single frequency component $\hat{V}^{(1)}$ in its Fourier transformation $\hat{V}^{(-1)}$. Assuming $[\hat{V}^{(1)}, \hat{V}^{(-1)}] = 0$, we obtain,

$$\hat{H}_{\text{eff}} = \hat{H}_0 - \frac{1}{2\omega^2} \left(\left[\hat{V}^{(1)}, \left[\hat{V}^{(-1)}, \hat{H}_0 \right] \right] + H.c. \right) + \mathcal{O} \left(\frac{1}{\omega^3} \right), \quad (\text{B18})$$

$$\hat{K}(t) = -\frac{i}{\omega} \left(\hat{V}^{(1)} e^{i\omega t} - \hat{V}^{(-1)} e^{-i\omega t} \right) - \frac{i}{\omega^2} \left(\left[\hat{V}^{(1)}, \hat{H}_0 \right] e^{i\omega t} - H.c. \right) + \mathcal{O} \left(\frac{1}{\omega^3} \right). \quad (\text{B19})$$

Interestingly, the first order terms of \hat{H}_{eff} vanish. As long as the potential is 1-local, \hat{H}_{eff} will also not grow in locality, making it implementable on quantum hardware without further compilation. Another simplification arises if

Property of \hat{H}_0	Property of $\hat{V}(t)$	Implications and implementation strategy	Form of \hat{H}_{eff} and $\hat{K}(t)$
$[\hat{H}_0, \hat{V}(t)] = 0 \forall t$	Single frequency	Trivial case. Standard Trotterization and the kick operator ansatz coincide.	(B22 - B23)
	Multiple frequencies	Different Fourier components $\hat{V}^{(j)}$ might not commute which creates effective dynamics.	(B20 - B21)
$[\hat{H}_0, \hat{V}(t)] \neq 0$	Single frequency	Corrections only from $[\hat{H}_0, \hat{V}(t)]$. This allows us to re-use previous time-independent techniques and lift them to Floquet Hamiltonian simulation.	(B18 - B19)
	Multiple frequencies	Most general case taking into account all effective dynamics.	(B16 - B17)

TABLE I. Comparison of special cases for the application to kick approximation

$[\hat{H}_0, \hat{V}(t)] = 0 \forall t$ or equivalently $[\hat{H}_0, \hat{V}^{(j)}] = [\hat{H}_0, \hat{V}^{(j)}] = 0 \forall j$. If we admit arbitrary potentials, we obtain,

$$\begin{aligned} \hat{H}_{\text{eff}} = & \hat{H}_0 + \frac{1}{\omega} \sum_{j=1}^{\infty} \frac{1}{j} [\hat{V}^{(j)}, \hat{V}^{(-j)}] - \frac{1}{3\omega^2} \sum_{j,k=1}^{\infty} \frac{1}{j(j+k)} \left([\hat{V}^{(j+k)}, [\hat{V}^{(-j)}, \hat{V}^{(-k)}]] + H.c. \right) \\ & - \frac{1}{3\omega^2} \sum_{j \neq k=1}^{\infty} \frac{1}{j(j-k)} \left([\hat{V}^{(j-k)}, [\hat{V}^{(-j)}, \hat{V}^{(k)}]] + H.c. \right) + \mathcal{O}\left(\frac{1}{\omega^3}\right), \end{aligned} \quad (\text{B20})$$

$$\begin{aligned} K(t) = & -\frac{i}{\omega} \sum_{j=1}^{\infty} \frac{1}{j} \left(\hat{V}^{(j)} e^{ij\omega t} - \hat{V}^{(-j)} e^{-ij\omega t} \right) - \frac{i}{2\omega^2} \sum_{j,k=1}^{\infty} \frac{1}{j(j+k)} \left([\hat{V}^{(j)}, \hat{V}^{(k)}] e^{i(j+k)\omega t} - H.c. \right) \\ & - \frac{i}{2\omega^2} \sum_{j \neq k=1}^{\infty} \frac{1}{j(j-k)} \left([\hat{V}^{(j)}, \hat{V}^{(-k)}] e^{i(j-k)\omega t} - H.c. \right) + \mathcal{O}\left(\frac{1}{\omega^3}\right). \end{aligned} \quad (\text{B21})$$

Here, \hat{H}_0 does not appear in higher order terms. This makes quantum simulation particularly simple, if the potential is 1-local since then $\hat{K}(t)$ and all corrections in \hat{H}_{eff} will be 1-local. For p -local \hat{V} , locality grows in general which introduces additional challenges for implementation. If both simplifications, $[\hat{H}_0, \hat{V}(t)] = 0$ and a single frequency driving with $[\hat{V}^{(j)}, \hat{V}^{(-j)}] = 0$, are given, the lowest order kick approximation becomes exact

$$\hat{H}_{\text{eff}} = \hat{H}_0 \quad (\text{B22})$$

$$\hat{K}(t) = -\frac{i}{\omega} \left(\hat{V}^{(1)} e^{i\omega t} - \hat{V}^{(-1)} e^{-i\omega t} \right). \quad (\text{B23})$$

Note that since $\hat{K}(t)$ just denotes an integration of $\hat{V}(t)$, we have reduced the kick approximation to a simple case of Trotterization.

In the third case of Table I, namely $[\hat{H}_0, \hat{V}(t)] \neq 0$ and a single frequency driving with $[\hat{V}^{(j)}, \hat{V}^{(-j)}] = 0$, a known implementation of the simulation under \hat{H}_0 comes in handy. Since the first order correction in \hat{H}_{eff} vanishes, simulating \hat{H}_0 alone already yields a good approximation to high frequency dynamics. In the simplest non-trivial case, \hat{H}_0 is diagonal as in the BNNNI model discussed in the main text. In that case, \hat{H}_0 can be simulated using a constant depth circuit. Similar cases of known implementations of \hat{H}_0 are 1D XY-models [28], Bethe diagonalizable models [71], and translational invariant models [34].

3. Leading error terms

Intimately related to the output fidelity is the Hilbert-Schmidt product of unitaries (cf. Eq. (10)), which we will focus on in the following error analysis. The error ξ which we derive in the following appears in the Hilbert-Schmidt product as follows $\text{Tr}\left(U_1^\dagger U_2\right) = d(1 - \xi)$ with the Hilbert space dimension d . In general, we have

$$\epsilon(\hat{U}_1, \hat{U}_2) = 1 - \frac{1}{d^2} \text{Tr}\left(\hat{U}_1^\dagger \hat{U}_2\right)^2 =: 1 - (1 - \xi)^2 = 2\xi + \mathcal{O}(\xi^2). \quad (\text{B24})$$

ξ can thus be seen as an estimate of the infidelity of a Haar random state undergoing evolution by \hat{U}_1 and \hat{U}_2 up to a factor of 2. Using permutation invariance of the trace, the Hilbert-Schmidt product between a kick approximation of first order and exact evolution reads

$$\text{Tr}\left(\hat{U}_{\text{exact}}^\dagger(t_0, t) \hat{U}_{\text{QHFFS}}(t_0, t)\right) = \text{Tr}\left(e^{i\tilde{K}(t_0)} e^{-i\hat{K}(t_0)} e^{i(t-t_0)\hat{H}_{\text{eff}}} e^{i\hat{K}(t)} e^{-i\tilde{K}(t)} e^{-i(t-t_0)\hat{H}_{\text{eff}}}\right), \quad (\text{B25})$$

where $\tilde{K}(t)$ denotes the truncated Kick operator and $\hat{K}(t)$ contains all orders (similar for \hat{H}_{eff}). As the trace of a commutator is always zero, $\text{Tr}\left([\hat{A}, \hat{B}]\right) = 0$, we will omit terms that contribute with a vanishing commutator term in what follows. We want to expand Eq. (B25) step-by-step in orders of $\frac{1}{\omega}$ starting with the exponentials of $\hat{K}(t)$ and $\tilde{K}(t)$. Using the Baker-Campbell-Hausdorff (BCH) lemma

$$e^{i\hat{K}(t)} e^{-i\tilde{K}(t)} = \mathbb{1} + i \frac{1}{\omega^2} \hat{K}^{(2)}(t) - \frac{1}{2\omega^4} \left(\hat{K}^{(2)}(t)\right)^2 + \mathcal{O}\left(\frac{1}{\omega^5}\right). \quad (\text{B26})$$

Since the kick operator, $\hat{K}(t)$, as well as the effective Hamiltonian, \hat{H}_{eff} , have a leading order error quadratic in $\frac{1}{\omega}$, which is a pure commutator, we expect the leading error of Eq. (B25) to be of fourth order (B25) as only products of commutators survive in the trace. The remaining factor will then be a similar combination of the exponentials of the effective Hamiltonians. This can be calculated with the following identity that follows from the Hadamard-Lemma

$$e^{\hat{A}} e^{-\hat{A} + \hat{\chi}} - \mathbb{1} = \int_0^1 ds e^{s\hat{A}} \hat{\chi} e^{-s\hat{A}} + \mathcal{O}(\hat{\chi}^2) = \sum_{q=0}^{\infty} \frac{1}{(q+1)!} [\hat{A}_{(q)}, \hat{\chi}] + \mathcal{O}(\hat{\chi}^2), \quad (\text{B27})$$

as before we denoted q -fold nested commutators by $[\hat{A}_{(q)}, \hat{\chi}] = [\hat{A}, [\hat{A}_{(q-1)}, \hat{\chi}]]$. Applied to the remaining factors of Eq. (B25), we define the second order error term of the effective Hamiltonian \hat{H}_{eff} as

$$\begin{aligned} e^{i(t-t_0)\hat{H}_{\text{eff}}} e^{-i(t-t_0)\hat{H}_{\text{eff}}} &= \mathbb{1} + \sum_{q=0}^{\infty} \frac{i^{q+1}(t-t_0)^{q+1}}{(q+1)!} \frac{1}{\omega^2} [\hat{H}_{0(q)}, \hat{H}_{\text{eff}}^{(2)}] + \mathcal{O}\left(\frac{1}{\omega^3}\right) \\ &=: \mathbb{1} + \hat{\Delta}_{\text{eff}}^{(2)}(t-t_0) + \mathcal{O}\left(\frac{1}{\omega^3}\right), \end{aligned} \quad (\text{B28})$$

where we used $\hat{A} := \hat{H}_{\text{eff}}$ and $\hat{\chi} = \hat{H}_{\text{eff}} - \tilde{H}_{\text{eff}}$. $\hat{\Delta}_{\text{eff}}$ again consists of commutators only and will consist of a series of infinitely many non-vanishing terms, in general. Later, we will use the integral formula (B27) to evaluate $\hat{\Delta}_{\text{eff}}^{(2)}$ for the model under consideration. Taking all factors together and plugging back into Eq. (B25), we obtain

$$\begin{aligned} \text{Tr}(\hat{U}_{\text{exact}}^\dagger(t_0, t) \hat{U}_{\text{QHIFFS}}(t_0, t)) &= d + \frac{1}{\omega^4} \text{Tr} \left(\frac{1}{2} \left(\hat{\Delta}_{\text{eff}}^{(2)}(t-t_0) \right)^2 - i\hat{K}^{(2)}(t_0) \hat{\Delta}_{\text{eff}}^{(2)}(t-t_0) - i\hat{K}^{(2)}(t) \hat{\Delta}_{\text{eff}}^{(2)}(t_0-t) + \right. \\ &\quad \left. + \hat{K}^{(2)}(t_0) e^{i(t-t_0)\hat{H}_0} \hat{K}^{(2)}(t) e^{-i(t-t_0)\hat{H}_0} - \frac{1}{2} \left(\hat{K}^{(2)}(t_0) \right)^2 - \frac{1}{2} \left(\hat{K}^{(2)}(t) \right)^2 \right) + \mathcal{O}\left(\frac{1}{\omega^5}\right), \end{aligned} \quad (\text{B29})$$

with $d = \text{Tr}(\mathbb{1})$ being the dimension of the Hilbert space. Note that, while $\hat{\Delta}_{\text{eff}}(t)$ is in general linear in the simulation time, t , the errors coming from the kick operator are constant amplitude oscillations. It is straightforward to generalize Eq. (B29) to higher order kick approximations. The general error term of a $(k-1)$ st order approximation reads

$$\begin{aligned} \text{Tr}(\hat{U}_{\text{exact}}^\dagger(t_0, t) \hat{U}_{\text{QHIFFS}}(t_0, t)) &= d + \frac{1}{\omega^{2k}} \text{Tr} \left(\frac{1}{2} \left(\hat{\Delta}_{\text{eff}}^{(k)}(t-t_0) \right)^2 - i\hat{K}^{(k)}(t_0) \hat{\Delta}_{\text{eff}}^{(k)}(t-t_0) \right. \\ &\quad \left. - i\hat{K}^{(k)}(t) \hat{\Delta}_{\text{eff}}^{(k)}(t-t_0) + \hat{K}^{(k)}(t_0) e^{it\hat{H}_0} \hat{K}^{(k)}(t) e^{-it\hat{H}_0} \right. \\ &\quad \left. - \frac{1}{2} \left(\hat{K}^{(k)}(t_0) \right)^2 - \frac{1}{2} \left(\hat{K}^{(k)}(t) \right)^2 \right) + \mathcal{O}\left(\frac{1}{\omega^{2k+1}}\right). \end{aligned} \quad (\text{B30})$$

With this general analysis, we find that the leading error term for high frequencies grows as

$$\text{Tr}(\hat{U}_{\text{exact}}^\dagger(t_0, t) \hat{U}_{\text{QHIFFS}}(t_0, t)) - d = \mathcal{O}\left(\frac{(t-t_0)^2}{\omega^{2k}} \alpha_{\text{comm}}^{(k)}\right). \quad (\text{B31})$$

$\alpha_{\text{comm}}^{(k)}$ includes norms of commutator terms that contain problem specific parameters.

4. Application to BNNNI

We will discuss the error of the approximated evolution of the BNNNI model in two dimensions that is introduced in Eq. (8) for $t_0 = 0$. The second order contributions of \hat{K} and \hat{H}_{eff} are

$$\hat{H}_{\text{eff}}^{(2)} = 2Jh^2 \left(\sum_{\langle\langle i,j \rangle\rangle} (\hat{Z}_i \hat{Z}_j - \hat{Y}_i \hat{Y}_j) + \kappa \sum_{\langle\langle i,j \rangle\rangle} (\hat{Z}_i \hat{Z}_j - \hat{Y}_i \hat{Y}_j) \right) + \mathcal{O}\left(\frac{1}{\omega^3}\right), \quad (\text{B32})$$

$$\hat{K}^{(2)}(t) = -2Jh \cos(\omega t) \left(\sum_{\langle\langle i,j \rangle\rangle} \hat{Y}_i \hat{Z}_j - \kappa \sum_{\langle\langle i,j \rangle\rangle} \hat{Y}_i \hat{Z}_j \right) + \mathcal{O}\left(\frac{1}{\omega^3}\right). \quad (\text{B33})$$

To calculate the terms involving $\hat{\Delta}_{\text{eff}}(t)$, we can apply the identity (B28). We will show the derivation of the quadratic term, the others vanish due to a mismatch of Pauli strings that are traceless. First, we use permutation invariance and change of integration variables to reduce the number of exponents in the expression

$$\frac{1}{2}\text{Tr}\left(\left(\hat{\Delta}_{\text{eff}}^{(2)}(t)\right)^2\right) = -\frac{1}{2}\text{Tr}\left(\int_0^t ds \int_{-s}^{t-s} du e^{-iu\hat{H}_0} \hat{H}_{\text{eff}}^{(2)} e^{iu\hat{H}_0} \hat{H}_{\text{eff}}^{(2)}\right). \quad (\text{B34})$$

Next, we simplify $e^{-iu\hat{H}_0} \hat{H}_{\text{eff}}^{(2)} e^{iu\hat{H}_0}$ under the integral. In the end, only Pauli strings that appear twice, once in $e^{-iu\hat{H}_0} \hat{H}_{\text{eff}}^{(2)} e^{iu\hat{H}_0}$ and once in \hat{H}_{eff} will have a non-vanishing trace. Considering this fact, we will gather irrelevant terms in the term $\hat{\zeta}$.

$$e^{-iu\hat{H}_0} \hat{H}_{\text{eff}}^{(2)} e^{iu\hat{H}_0} = 2Jh^2 \left(\sum_{\langle i,j \rangle} \hat{Z}_i \hat{Z}_j + \kappa^2 \sum_{\langle\langle i,j \rangle\rangle} \hat{Z}_i \hat{Z}_j - \cos^6(2Ju) \cos^6(2J\kappa u) \left(\sum_{\langle i,j \rangle} \hat{Y}_i \hat{Y}_j + \kappa^2 \sum_{\langle\langle i,j \rangle\rangle} \hat{Y}_i \hat{Y}_j \right) \right) + \hat{\zeta}, \quad (\text{B35})$$

While the terms $\hat{Z}_i \hat{Z}_j$ commute with \hat{H}_0 and therefore stay unchanged, the $\hat{Y}_i \hat{Y}_j$ terms will collect factors from every non-commuting term in \hat{H}_0 . The cos factors are derived using the identity for the exponential of a Pauli string \hat{P} : $e^{i\theta\hat{P}} = \cos\theta\hat{1} + i\sin\theta\hat{P}$. Plugging back into Eq. (B34), we get a dominant quadratic term $\frac{281}{64}J^2h^2(1+\kappa^2)t^2$ followed by a series of oscillatory terms that do not scale in time. Plugging $\hat{K}^{(2)}(t)$ into the remaining terms of Eq. (B29) yields

$$\begin{aligned} \frac{\omega^4}{nh^2} \left(1 - \frac{1}{d} \text{Tr}(\hat{U}_{\text{exact}}^\dagger(t) \hat{U}_{\text{QHIFFS}}(t)) \right) = & h^2(1+\kappa^2) \left(\frac{281}{64}J^2t^2 + \frac{75\sin^2(2Jt)}{512} + \frac{15\sin^2(4Jt)}{1024} + \frac{\sin(6J(1+\kappa)t)^2}{18432(1+\kappa)^2} \right. \\ & + \frac{5\sin^2(6Jt)}{4608} + \frac{15\sin^2(2J(-3+\kappa)t)}{2048(\kappa-3)^2} + \frac{45\sin^2(2J(-2+\kappa)t)}{1024(\kappa-2)^2} + \\ & + \frac{225\sin^2(2J(-1+\kappa)t)}{2048(\kappa-1)^2} + \frac{9\sin(4J(-1+\kappa)t)^2}{2048(-1+\kappa)^2} + \frac{\sin(6J(-1+\kappa)t)^2}{18432(-1+\kappa)^2} + \\ & + \frac{75\sin(2J\kappa t)^2}{512\kappa^2} + \frac{15\sin(4J\kappa t)^2}{1024\kappa^2} + \frac{5\sin(6J\kappa t)^2}{4608\kappa^2} + \frac{225\sin(2J(1+\kappa)t)^2}{2048(1+\kappa)^2} + \\ & + \frac{9\sin(4J(1+\kappa)t)^2}{2048(1+\kappa)^2} + \frac{45\sin(2J(2+\kappa)t)^2}{1024(2+\kappa)^2} + \frac{15\sin(2J(3+\kappa)t)^2}{2048(3+\kappa)^2} + \\ & + \frac{3\sin(2J(-3+2\kappa)t)^2}{1024(3-2\kappa)^2} + \frac{45\sin(2J(-1+2\kappa)t)^2}{1024(1-2\kappa)^2} + \frac{45\sin(2J(1+2\kappa)t)^2}{1024(1+2\kappa)^2} + \\ & + \frac{3\sin(2J(3+2\kappa)t)^2}{1024(3+2\kappa)^2} + \frac{3\sin(2J(-2+3\kappa)t)^2}{1024(2-3\kappa)^2} + \frac{15\sin(2J(-1+3\kappa)t)^2}{2048(1-3\kappa)^2} + \\ & + \frac{15\sin(2J(1+3\kappa)t)^2}{2048(1+3\kappa)^2} + \frac{3\sin(2J(2+3\kappa)t)^2}{1024(2+3\kappa)^2} \left. \right) + 8J^2(1+\cos^2(\omega t))(1+\kappa^2) \\ & - 16J^2\cos(\omega t)\cos^2(2Jt)\cos^4(2J\kappa t)\left((1+\kappa^2)\cos^2(2Jt) - 3\sin(J\kappa t)\right). \quad (\text{B36}) \end{aligned}$$

This expression for the QHiFFS error (using a 1st-order effective Hamiltonian and kick approximation) is exact to corrections in $\mathcal{O}\left(\frac{1}{\omega^6}\right)$. We plot it in full in Fig. 4(a-c). At long times the first term, which grows quadratically in t , dominates leading to the approximate scaling quoted in Eq. (12) in the main text. Note that Eq. (B36) also encodes the error of an Ising model, which can be computed taking the limit $\kappa \rightarrow 0$. The linear factor n above accounts for the number of interaction terms for our local Hamiltonian. Note that, in general, long range interactions can exhibit a maximal error scaling quadratically in n .

	Next-nearest neighbor Ising (NNNI)			Nearest neighbor Ising (NNI)		
D	1	2	3	1	2	3
$2n_n$	2	6	10	2	6	10
c_{t^2}	2.5	$\frac{281}{64} \approx 4.39$	$\frac{208515}{32768} \approx 6.36$	3	5.25	$\frac{957}{128} \approx 7.48$

TABLE II. List of error coefficients $c_{t^2} = 2D(1 + c_{1,1,n_1,n_2}^\kappa)$, defined implicitly in Eq. (B37), applied to one-, two-, and three-dimensional ($D = 1, 2, 3$) nearest neighbour Ising (NNI) and next-nearest neighbour Ising (NNNI) models. Note that the BNNNI model corresponds to a 2D NNNI model. $2n_n$ is the number of mutually non-commuting Hamiltonians in $H_{\text{eff}}^{(2)}$.

5. Dependence on dimension and locality

Here we focus on the BNNNI model interaction type ($\hat{Z}\hat{Z}$) with periodic driving and alter spatial dimension, D , and locality of the interaction that will finally influence the number of mutually non-commuting Hamiltonians in $\hat{H}_{\text{eff}}^{(2)}$, $2n_n$. Most interesting for long times will be the quadratically scaling error term of the form

$$\xi = c_{t^2} \frac{nJ^2 h^4}{\omega^4} (1 + \kappa^2) t^2 + o(t) \quad (\text{B37})$$

The coefficient c_{t^2} comes out of the integral in Eq. (B34). We want to generalize this expression in the following to arbitrary spatial dimensions D that will leave the Hamiltonian the same but changes the number of nearest and next-nearest neighbor terms. The following derivation is straight-forwardly generalized to p -local $\hat{Z}^{\otimes p}$ interactions because c_{t^2} only depends on the number of non-commuting terms for a fixed \hat{Y} -interaction in $H_{\text{eff}}^{(2)}$ each contributing with a cosine factor in Eq. (B34). In this analysis, we assume the number of mutually non-commuting Hamiltonians to be even; as for an odd number of cosine factors, the integral vanishes. The coefficient of the dominant (linear) term of the inner integral of Eq. (B34) will then reduce to

$$c_{t^2} = 2D \left(1 + \lim_{s \rightarrow \infty} \frac{1}{s} \int_0^s du \cos(2u)^{2n_n} \cos(2\kappa u)^{2n_n} \right), \quad (\text{B38})$$

where the factor D comes from the fact that the number of interaction terms scales linearly in the spatial dimension. The 1 in the brackets resembles the coefficient of the $\hat{Z}\hat{Z}$ interactions and the integral comes from the $\hat{Y}\hat{Y}$ interactions. The integral in Eq. (B38) can be calculated assuming $\kappa \neq 1$ using a recursive formula. First define

$$c_{a_1, a_2, n_1, n_2}^\kappa := \lim_{s \rightarrow \infty} \frac{1}{s} \int_0^s du \cos(2^{a_1} u)^{2n_1} \cos(2^{a_2} \kappa u)^{2n_2}. \quad (\text{B39})$$

Using the trigonometric identity $\cos^2 x = \frac{1}{2}(1 + \cos(2x))$ and the binomial theorem, we can write down relations between the coefficients

$$c_{a_1, a_2, n_1, n_2}^\kappa := \frac{1}{2^{n_1+n_2}} \sum_{x_1=0}^{\lfloor \frac{n_1}{2} \rfloor} \sum_{x_2=0}^{\lfloor \frac{n_2}{2} \rfloor} \binom{n_1}{2x_1} \binom{n_2}{2x_2} c_{a_1+1, a_2+1, x_1, x_2}^\kappa. \quad (\text{B40})$$

These can now be recursively calculated using the termination conditions $c_{a_1, a_2, 0, 0} = 1$ and $c_{a_1, a_2, 0, 1} = c_{a_1, a_2, 1, 0} = \frac{1}{2}$. Plugging in the data of a two-dimensional BNNNI model ($D = 2, 2n_n = 2n_1 = 2n_2 = 6$) into Eq. (B40) indeed yields the coefficient $\frac{281}{64}$ that is consistent with Eq. (B36). We have gathered a number of examples in Table II.

Note that in the limit of large D , the complicated integral contribution of Eq. (B38) is vanishing making the dependence on D asymptotically linear. Putting this together with Eq. (B31), we can write down the scaling of the dominant error term of a second order kick approximation of the BNNNI model

$$\text{Tr}(\hat{U}_{\text{exact}}^\dagger(t) \hat{U}_{\text{QHFFS}}(t)) - d = \mathcal{O} \left(\frac{t^2}{\omega^4} J^2 h^4 n D (1 + o(1)) \right), \quad (\text{B41})$$

where $o(1)$ denotes a term that vanishes in the limit of large D .

C. Derivation of Trotterization error estimate

To compare to standard methods of quantum simulation, we give an upper bound for the error of first order Trotter formulas,

$$\hat{U}_{\text{Trotter}}(t_0, t) = \prod_{r=1}^m \prod_{j=1}^J e^{i\delta t \hat{H}_j(t_0+r\delta t)}, \quad (\text{C1})$$

where $\hat{H}(t) = \sum_{j=1}^J \hat{H}_j(t)$ is a choice of Hamiltonian decomposition and $\delta t = \frac{t-t_0}{m}$. Standard Trotter errors come from the non-commutativity of the Hamiltonians \hat{H}_j . As the Hamiltonian of interest is time-dependent, there are two other sources of error coming from the non-commutativity of the Hamiltonian at different times and the discretization of the time-ordered integrals that is implicit in Eq. (C1). Using the triangle inequality, the error is bounded by

$$\begin{aligned} \left\| \mathcal{T} e^{-i \int_{t_0}^t \hat{H}(s) ds} - \hat{U}_{\text{Trotter}}(t_0, t) \right\| &\leq \left\| \mathcal{T} e^{-i \int_{t_0}^t \hat{H}(s) ds} - e^{-i \int_{t_0}^t \hat{H}(s) ds} \right\| + \left\| e^{-i \int_{t_0}^t \hat{H}(s) ds} - \hat{U}_{\text{disc}}(t_0, t) \right\| \\ &+ \left\| \hat{U}_{\text{disc}}(t_0, t) - \hat{U}_{\text{Trotter}}(t_0, t) \right\| =: \xi_1 + \xi_2 + \xi_3, \end{aligned} \quad (\text{C2})$$

$$\text{with } \hat{U}_{\text{disc}}(t_0, t) = \prod_{r=1}^m e^{i\delta t \hat{H}(t_0+r\delta t)}. \quad (\text{C3})$$

The first term, ξ_1 , in Eq. (C2) describes errors from the non-commutativity of $\hat{H}(t)$ at different times scaling with $\max_{s,s'} [\hat{H}(s), \hat{H}(s')]$, the second term, ξ_2 , takes into account the discretization of the integral and the third term, ξ_3 , is the standard Trotter error scaling with commutators $[\hat{H}_i, \hat{H}_j]$. $\xi_1 + \xi_3$ scales as $\mathcal{O}\left(\frac{t}{m} J(1 + \kappa) h\right)$ for the BNNNI model. We will see that in the regime of large frequencies, ω , the term ξ_2 will be dominant. Since, we are interested in the 2-norm squared, there will also be mixed terms taking into account ξ_1, ξ_2, ξ_3 .

For the sake of clarity we will now focus on ξ_2 only. To do so, we neglect the non-commutativity for a moment and consider just a time-discretization as described in Eq. (C3). If we neglect the non-commutativity of the Hamiltonian at different times $[\hat{H}(s), \hat{H}(s')] = 0$, we can write the generator of discretized dynamics with the Heavyside step function $\Theta(x) = \begin{cases} 0 & x < 0 \\ 1 & x \geq 0 \end{cases}$

$$\left\| \hat{U}_{\text{exact}}(t_0, t) - \hat{U}_{\text{disc}}(t_0, t) \right\|^2 = \left\| e^{-i \int_{t_0}^t \hat{H}(s) ds} - e^{-i \int_{t_0}^t \hat{H}_{\text{disc}}(s) ds} \right\|^2 \quad (\text{C4})$$

$$\text{with } \hat{H}_{\text{disc}}(s) = \sum_{r=1}^m (\Theta(s - (r-1)\delta t) - \Theta(s - r\delta t)) \hat{H}(r\delta t). \quad (\text{C5})$$

Using the inequality $\|e^{i\hat{H}_1} - e^{i\hat{H}_2}\| \leq \|\hat{H}_1 - \hat{H}_2\|$ (see Lemma 50 of Ref. [98] for proof), we get:

$$\left\| \hat{U}_{\text{exact}}(t_0, t) - \hat{U}_{\text{disc}}(t_0, t) \right\|^2 \leq \left\| \int_{t_0}^t ds \hat{H}(s) - \delta t \sum_{r=1}^m \hat{H}(t_0 + r\delta t) \right\|^2 \quad (\text{C6})$$

The 2-norm can be related to the Hilbert-Schmidt product via $\frac{1}{2d} \|\hat{U}_1 - \hat{U}_2\|^2 = 1 - \frac{1}{d} \text{Re}(\text{Tr}(\hat{U}_1^\dagger \hat{U}_2))$, so that the two measures can be directly compared, as $\text{Tr}(\hat{U}_1^\dagger \hat{U}_2)$ is real by construction.

For the BNNNI model, only the oscillating terms will survive in Eq. (C6). As we are integrating over a cosine, integrations over every full period vanish. Coarse discretizations, however, will collect error terms. We divide the

time interval $t - t_0 = lT + \delta$, $l \in \mathbb{N}$ into an interval of l full periods and $\delta < T$.

$$\left\| \hat{U}_{\text{exact}}(t_0, t) - \hat{U}_{\text{disc}}(t_0, t) \right\|^2 \leq h^2 \left\| \sum_j \hat{X}_j \right\|^2 \left| \int_{t_0}^t ds \cos(\omega s) - \delta t \sum_{r=1}^m \cos(\omega(t_0 + r\delta t)) \right|^2 + \mathcal{O}(\delta t^2) \quad (\text{C7})$$

$$\leq h^2 n d \left| \int_{t-\delta}^t ds \cos(\omega s) - \delta t \sum_{r=m-m_\delta+1}^m \cos(\omega(t_0 + r\delta t)) - l\delta t \max_{l \in [0, \dots, m-1]} \sum_{r=\frac{l}{k}(m-m_\delta)+1}^{\frac{l+1}{l}(m-m_\delta)} \cos(\omega(t_0 + r\delta t)) \right|^2. \quad (\text{C8})$$

Here, we assume the number of Trotter steps, m , to be equally divided over the time interval which leaves m_δ steps for simulation $s \in [lT, lT + \delta]$ and $m - m_\delta$ for the simulation of l full periods. The last term of Eq. (C8) describes the worst discretization of the l period which yields an upper bound for every other period. Standard estimates of the Riemann sum errors give,

$$\begin{aligned} \frac{1}{2d} \left\| \hat{U}_{\text{exact}}(t_0, t) - \hat{U}_{\text{disc}}(t_0, t) \right\|^2 &\leq \frac{h^2 n}{2} \left(\frac{T^2 \omega m^2}{2(m - m_\delta)} \max_{s \in [0, T]} |\sin(\omega s)| + \frac{\delta^2 \omega}{2m_\delta} \max_{s \in [0, \delta]} |\sin(\omega s)| \right)^2 \\ &\leq \frac{h^2 \pi^2 n}{2} \left(\frac{Tm^2}{m - m_\delta} + \frac{\delta}{m_\delta} \right)^2 \end{aligned} \quad (\text{C9})$$

$$= \frac{h^2 \pi^2 n (t - t_0)^2}{2m^2} (m + 1)^2 = \frac{h^2 n (t - t_0)^2}{2m^2} \left((t - t_0 - \delta) \frac{\omega}{2} + \pi \right)^2. \quad (\text{C10})$$

In the last three steps, we further estimated $|\sin x| \leq 1$, $\delta \leq T$ and plugged in $\omega = \frac{2\pi}{T}$ and $\frac{m_\delta}{m} = \frac{\delta}{t-t_0}$, as well as $\frac{m-m_\delta}{l} = \frac{lT}{t-t_0}$ coming from the equal distribution of Trotter steps. Finally, we expressed the number of periods $l = (t - t_0 - \delta) \frac{\omega}{2\pi}$ and the period, T , in terms of the driving frequency, ω . In the special case $\delta = 0$, we can absorb the second term of Eq. (C10) in l . The error then reads

$$\frac{1}{2d} \left\| \hat{U}_{\text{exact}}(t_0, t) - \hat{U}_{\text{disc}}(t_0, t) \right\|^2 \leq \frac{h^2 n}{8m^2} (t - t_0)^4 \omega^2. \quad (\text{C11})$$

Note the quadratic dependence on ω that makes ξ_2 the dominant error in our setting. If both kick and Trotter approximations have comparable error, the Trotter number, m , can be bounded

$$\begin{aligned} (\text{C11}) \stackrel{!}{=} (\text{B36}) &\iff \frac{h^2 n}{m^2} t^4 \omega^2 \geq \frac{281}{8} \frac{J^2 h^4 n}{\omega^4} (1 + \kappa^2) t^2 + \mathcal{O}\left(\frac{1}{\omega^4}\right) + \mathcal{O}\left(\frac{t^2}{\omega^6}\right) \\ &\iff m \leq \frac{t\omega^3}{Jh\sqrt{1 + \kappa^2} + \mathcal{O}\left(\frac{1}{t}\right) + \mathcal{O}\left(\frac{1}{\omega}\right)} \\ &\implies m = \mathcal{O}\left(\frac{t\omega^3}{Jh\sqrt{1 + \kappa^2}}\right) = R. \end{aligned} \quad (\text{C12})$$

We have set $t_0 = 0$ for comparison without loss of generality. For the sake of simplicity, we have chosen the best case $\delta = 0$ for the Trotter sequence, so the second term of Eq. (C10) is dropped. Also note that Eq. (C12) only holds in the high-frequency regime in which Eq. (B36) is a good estimate and Eq. (C11) is the dominant Trotter error. Finally, since the 1st. order QHiFFS requires the same number of two qubit gates as one (1st. or 2nd. order) Trotter step, we have here that $m = R$ where R is the ratio of the number of two-qubit gates required by standard Trotterization compared to QHiFFS to implement a simulation of the same fidelity.